cPLA2α and EHD1 interact and regulate the vesiculation of cholesterol-rich, GPI-anchored, protein-containing endosomes

Bishuang Cai, Steve Caplan, and Naava Naslavsky
Department of Biochemistry and Molecular Biology, University of Nebraska Medical Center, Omaha, NE 68198

ABSTRACT **The lipid modifier phospholipase A2 catalyzes the hydrolysis of phospholipids to inverted-cone–shaped lysophospholipids that contribute to membrane curvature and/or tubulation. Conflicting findings exist regarding the function of cytosolic phospholipase A2 (cPLA2) and its role in membrane regulation at the Golgi and early endosomes. However, no studies addressed the role of cPLA2 in the regulation of cholesterol-rich membranes that contain glycosylphosphatidylinositol-anchored proteins (GPI-APs). Our studies support a role for cPLA2α in the vesiculation of GPI-AP–containing membranes, using endogenous CD59 as a model for GPI-APs. On cPLA2α depletion, CD59-containing endosomes became hypertubular. Moreover, accumulation of lysophospholipids induced by a lysophospholipid acyltransferase inhibitor extensively vesiculated CD59-containing endosomes. However, overexpression of cPLA2α did not increase the endosomal vesiculation, implying a requirement for additional factors. Indeed, depletion of the "pinchase" EHD1, a C-terminal Eps15 homology domain (EHD) ATPase, also induced hypertubulation of CD59-containing endosomes. Furthermore, EHD1 and cPLA2α demonstrated in situ proximity (<40 nm) and interacted in vivo. The results presented here provide evidence that the lipid modifier cPLA2α and EHD1 are involved in the vesiculation of CD59-containing endosomes. We speculate that cPLA2α induces membrane curvature and allows EHD1, possibly in the context of a complex, to sever the curved membranes into vesicles.**

Monitoring Editor
Jean E. Gruenberg
University of Geneva

Received: Oct 27, 2011
Revised: Feb 22, 2012
Accepted: Mar 19, 2012

INTRODUCTION

Intracellular trafficking requires the constant formation of carrier vesicles. These vesicles, which bud from the donor membrane, detach and move toward their destination organelle and subsequently fuse with it. Vesicle generation is one of the most active membrane-shaping processes in the cell and necessitates major membrane deformation that cannot occur spontaneously. An energy barrier has to be surpassed in order to reshape the bilayer equilibrium into a highly curved membrane (Grimmer *et al.*, 2005; Kooijman *et al.*, 2005).

Membrane remodeling is facilitated by two key mechanisms: 1) protein-induced membrane curvature and 2) lipid-based bilayer asymmetry. Constriction of the membrane toward the formation of a budding vesicle with the assistance of *proteins* is complex and often includes an array of proteins that, in concerted activity, create curvature by mechanically bending the bilayer either by inserting their tail portion into the leaflet or by oligomerizing in a scaffolding coat-like manner (Graham and Kozlov, 2010). Lipid-mediated curvature can be achieved when cone-shaped or inverted-cone–shaped lipids are packed locally in a monolayer leaflet, driving leaflet asymmetry into positive or negative curvature. These deep invagination areas, often known as the neck, eventually undergo scission as the last step in vesicle formation (Kooijman *et al.*, 2003).

Scission is performed by a number of proteins, often operating as complexes such as the GTPase dynamin (Lenz *et al.*, 2009) with its binding partners and the endosomal sorting complex required for transport (ESCRT) proteins (Hurley and Hanson, 2010). It was proposed that constriction of certain cholesterol-containing tubular plasma membrane invaginations can be driven by domain boundary forces and be reorganized by actin in a process that leads to scission

This article was published online ahead of print in MBoC in Press (http://www.molbiolcell.org/cgi/doi/10.1091/mbc.E11-10-0881) on March 28, 2012.

Address correspondence to: Naava Naslavsky (nnaslavsky@unmc.edu).

Abbreviations used: cPLA2, cytosolic phospholipase A2; EHD, Eps15 homology domain; GPI-AP, glycosylphosphatidylinositol-anchored protein; LPAT, lysophospholipid acyltransferase; LPL, lysophospholipid; MAFP, methyl arachidonyl fluorophosphonate; PA, phosphatidic acid; PL, phospholipid; PM, plasma membrane.

(Romer *et al.*, 2010). Together, enzymes, bending/scission proteins, and cytoskeletal elements might bring about the formation of a new budding vesicle.

Recently there has been increasing interest in enzymatic lipid modifications that drive membrane asymmetry as important factors in initiating vesicle formation. Several enzymes are known to affect membrane trafficking, among them the Ca^{2+}-dependent cytosolic phospholipase A2 (group IV, PLA2α; reviewed in Brown *et al.*, 2003). The PLA2 superfamily has historically been implicated in the formation of signaling molecules such as arachidonic acid, and therefore it was extensively studied in the context of signal transduction. However, in recent years researchers have begun to assess the role of this enzyme in the regulation of membrane trafficking. As a lipid modifier, PLA2 may act locally to remodel membrane curvature, thus regulating vesiculation and tubulation dynamics. PLA2 is recruited to membrane-residing phospholipids, where it catalyzes the hydrolysis of glycerophospholipid at its *sn*-2 ester bond, giving rise to a free fatty acid and lysophospholipid (LPL), an inverted-cone–shaped lipid that triggers positive curvature in the membrane leaflet. Lysophosphatidic acid (LPA), which is a form of LPL frequently found in biological membranes, can be further converted into the cylindrical-shaped phosphatidic acid (PA) by proteins with lysophosphatidic acid acyltransferase activity (reviewed in Brown *et al.*, 2003).

A growing number of studies have shown that vesicles, budding from the plasma membrane via different pathways of internalization, may maintain distinct itineraries throughout their intracellular trafficking (Mayor *et al.*, 1998). It was suggested that the basis for this distinction might lie in part with the lipid composition of the membranes. Proteins with affinity to specific lipids/phospholipids might provide the sorting and targeting elements that further distinguish the routes and itineraries for such vesicles, creating subpopulations of endosomes. Cholesterol was described repeatedly as a lipid that influences trafficking. Its partitioning into microdomains at the plasma membrane (PM) and endosome and Golgi membranes renders it an important factor that can determine the kinetics and destination of the transport vesicle (Brown *et al.*, 2003; Llorente *et al.*, 2007; Sandvig *et al.*, 2008; Lewis and Hooper, 2011; Reverter *et al.*, 2011).

Because increasing cholesterol levels in the Golgi stacks induce recruitment and activation of cytosolic phospholipase A2α (cPLA2α), triggering aberrant vesiculation of the Golgi (Grimmer *et al.*, 2005), we assessed the contribution of this enzyme to the process of vesiculation and tubulation of endosomes, in particular those containing glycosylphosphatidylinositol-anchored protein (GPI-AP), also termed GEEC (Sabharanjak *et al.*, 2002). cPLA2 and caveolin1, a cholesterol-binding protein and a major scaffolding in caveolae, were previously found to coimmunoprecipitate in mouse hippocampal neurons (Gaudreault *et al.*, 2004). Moreover, activation of cPLA2 was directly linked to the transport of the prion protein peptide PrP82-146 via the cholesterol-rich rafts pathway, thereby affecting its metabolism (Bate *et al.*, 2011).

In addition, bacterial toxins (Montesano *et al.*, 1982; Moya *et al.*, 1985; Sandvig and van Deurs, 1994), as well as viruses (Madshus *et al.*, 1987) and major histocompatibility class I (Naslavsky *et al.*, 2004) and GPI-AP molecules (Sabharanjak *et al.*, 2002; Mayor and Riezman, 2004), internalize via the clathrin-independent pathway and are often taken up in deep invaginating tubules originating at the PM (Massol *et al.*, 2005). These structures contain a significant level of cholesterol that is maintained throughout the endocytic pathway (Mayor *et al.*, 1998; Gagescu *et al.*, 2000). Some of these bacterial toxins can even induce the formation of membrane tubules that pinch off in a dynamin-dependent manner, hence mediating their own uptake (Romer *et al.*, 2007).

Our previous work showed that GPI-AP–containing endosomes partially associate with the C-terminal Eps15 homology domain 1 protein (EHD1), which regulates their transport to the recycling compartment in a protein kinase C–dependent manner (Cai *et al.*, 2011). In the present study we demonstrate that EHD1 and cPLA2α interact in vivo and may cooperate in the process of endosome vesiculation formed within the clathrin-independent pathway.

RESULTS

Potential role for cPLA2α vesiculation of GPI-AP–containing endosomes

Because cholesterol has been implicated in the recruitment of cPLA2 to Golgi membranes (Grimmer *et al.*, 2005), we investigated the involvement of cPLA2 in the generation of GPI-AP–containing endosomes, shown previously to contain high levels of cholesterol (Gagescu *et al.*, 2000; Maxfield and Wustner, 2002; Sabharanjak *et al.*, 2002; Edidin, 2003; Naslavsky *et al.*, 2004; Sharma *et al.*, 2004). We chose to knock down the cytosolic Ca^{2+}-dependent PLA2α (cPLA2α, group IV), which was recently described as a modulator of the Golgi stacks (San Pietro *et al.*, 2009). To ensure that our anti-cPLA2α antibody specifically recognized this particular isoform, we first transfected HeLa cells with hemagglutinin (HA)-cPLA2α and demonstrated that a band corresponding to cPLA2α was detected by both anti-HA and anti-cPLA2α antibodies (Figure 1, lanes 1 and 2 respectively). We then knocked down the *endogenous* cPLA2α with small interfering RNA (siRNA) treatment. As demonstrated in lanes 5 and 6, >90% reduction of endogenous cPLA2α was observed upon siRNA treatment and by immunoblotting with anti-cPLA2α antibodies. A similar reduction was also observed in HA-cPLA2α–expressing cells, as detected by anti-cPLA2α antibody (Figure 1, lanes 3 and 4). This experiment also indicated that HeLa cells express endogenous cPLA2α (Figure 1, lane 5).

We previously showed that within minutes of antibody-induced internalization, the GPI-AP CD59 localizes to tubulovesicular structures that partially costain with EHD1 (Cai *et al.*, 2011). To determine whether cPLA2α affects the generation of these endosomes, we depleted HeLa cells of cPLA2α and examined the morphology of CD59-containing endosomes after a brief internalization of 3 min. As demonstrated, the knockdown of cPLA2α caused a significant level of hypertubulation of CD59-containing endosomes compared with mock-treated cells (Figure 1, compare C to B). This hypertubulation was also observed after longer periods of CD59 internalization (10–30 min) upon cPLA2α depletion. Scoring cells with tubular CD59 endosomes under these conditions revealed a threefold increase in the number of cells with this phenotype (Figure 1I). We also observed that these tubular structures are longer and more elaborate than those in mock-treated cells. At higher magnification and when visualized with green fluorescent protein (GFP)-myc-EHD1 (Figure 1D), endogenous MICAL-L1 (unpublished data) or both (Supplemental Figure S2A), these aligned CD59 punctae are seen as part of a continuous tubular structure. Blue arrows depict continuous CD59 tubules decorated by EHD1, and yellow arrows point to CD59 punctae within a continuous EHD1-decorated tubule—a more common feature observed postfixation. The "beads-on-a-string" appearance of CD59-containing tubular endosomes is likely acquired as a result of the fixation protocol because during live-imaging analysis of internalizing endogenous CD59, this cargo is observed on continuous tubular structures (see Supplemental Figure 2 in Cai *et al.*, 2011).

Of importance, the enhanced hypertubulation seen with CD59 was specific for cPLA2α-depletion, as reintroduction of a siRNA-resistant cPLA2α cDNA no longer culminated in excessive tubulation

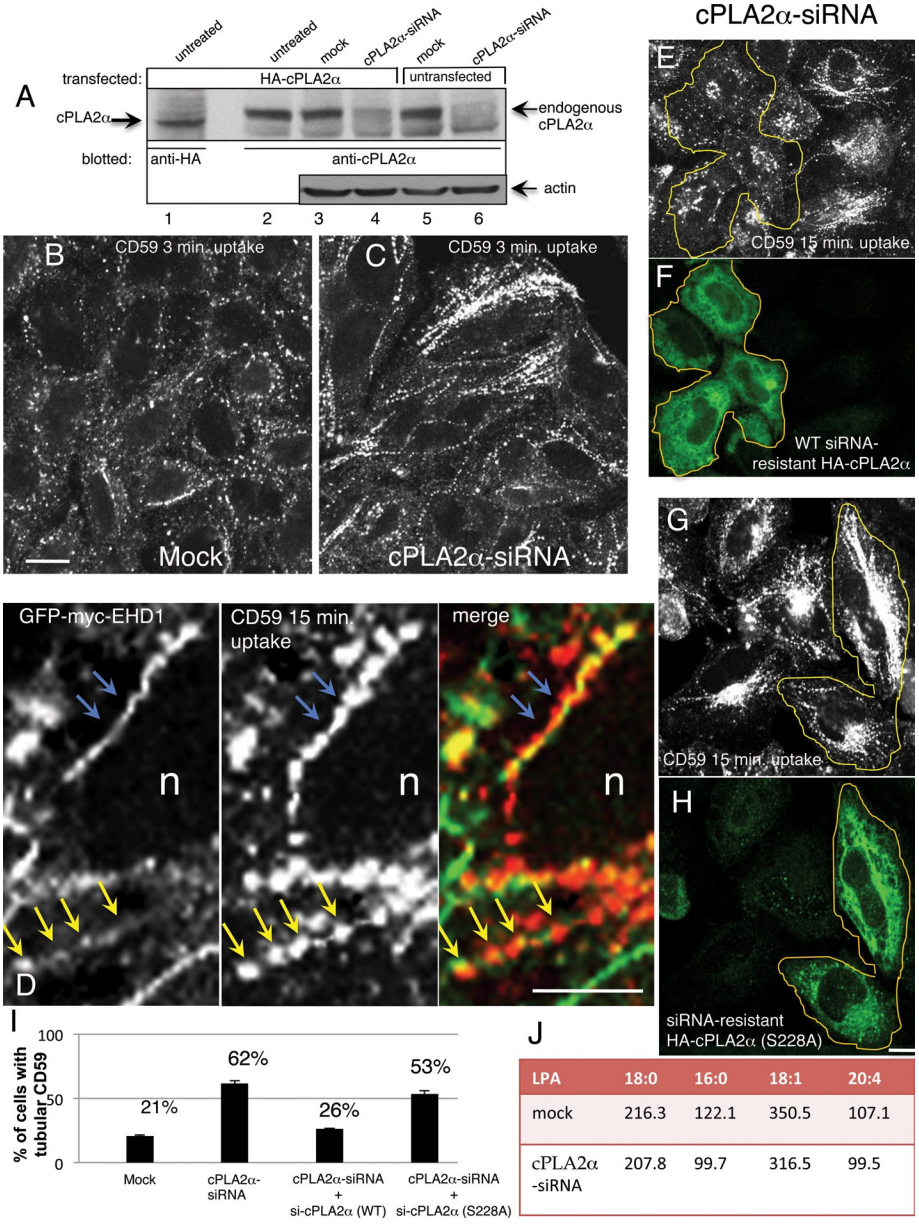

J

LPA	18:0	16:0	18:1	20:4
mock	216.3	122.1	350.5	107.1
cPLA2α -siRNA	207.8	99.7	316.5	99.5

FIGURE 1: Depletion of cPLA2α induces hypertubulation of CD59-containing endosomes. (A) Untransfected (lanes 5 and 6) or HA-cPLA2α–overexpressing HeLa cells (lanes 1–4) were mock treated (lanes 3 and 5) or treated with cPLA2α-siRNA for 2 d (lanes 4 and 6), harvested, and lysed. Lysates were separated by 8% SDS–PAGE, transferred to nitrocellulose filters, and immunoblotted with either mouse anti-HA antibody (lane 1, to identify the band corresponding to the particular α isoform of cPLA2) and anti-cPLA2α antibody (lanes 2–6, to detect endogenous and overexpressed cPLA2α). Actin was probed as a protein loading control (lanes 3–6). Note that a band corresponding to both overexpressed and endogenous cPLA2α is greatly reduced by the siRNA treatment (lanes 4 and 6). (B, C) HeLa cells growing on coverslips were mock treated (B) or treated with cPLA2α–siRNA (C). After 48 h, cells were incubated with mouse anti-CD59 antibody for 3 min at 37°C, acid stripped, and fixed. Internalized CD59 was detected with Alexa 568–conjugated anti-mouse antibody. (D) High magnification of tubular interconnected "beads-on-a-string" endosome. HeLa cells transfected with GFP-myc-EHD1 were allowed to internalize anti-CD59 for 15 min at 37°C, then acid stripped, fixed, and stained with Alexa 568 goat anti-mouse secondary antibody. Blue arrows depict continuous CD59 and EHD1 tubules, and yellow arrows point to the postfixation commonly seen CD59 "beads" within the continuous EHD1-decorated tubular membrane. (E–H) Either siRNA-resistant wild-type HA-cPLA2α (E, F) or active-site mutant (S228A) (G, H) was transfected into cPLA2α-siRNA–treated cells. After 48 h, cells were pulsed with anti-CD59 antibody for 15 min, acid stripped, and fixed. Cells were then stained with rabbit anti-HA antibody to identify cPLA2α-expressing cells, denoted with yellow lines, followed by Alexa 568–conjugated anti-mouse and Alexa 488–conjugated anti-rabbit antibody. (I) Quantification of the percentage of cells with tubular CD59 for mock-treated, cPLA2α-siRNA–treated, and rescue-treated cells by transfecting cells with either siRNA-resistant wild-type HA-cPLA2α or S228A mutant. This experiment was repeated three times, and SE is shown. (J) Cells were either mock treated or treated with cPLA2α-siRNA for 48 h and then scraped and spun down. A small sample of each cell pellet was sonicated and subjected to total protein measurement, whereas the rest of the cell pellet was extracted with acidified 1-butanol (see *Materials and Methods*). Saturated (18:0, 16:0) and unsaturated (18:1, 20:4) LPA species were analyzed by liquid chromatography–tandem mass spectrometry. Data presented represents the average of two independent experiments, and the concentration of each LPA species is given in ng LPA/mg protein. Bar, 10 μm.

of CD59-containing endosomes (Figure 1, E and F, quantified in I; the yellow border denotes cells expressing siRNA-resistant cPLA2α). Moreover, an inactive form of cPLA2α (S228A), mutated in its active site (Sharp *et al.*, 1994), failed to rescue the siRNA-treated cells and preserved the hypertubular CD59 phenotype (Figure 1, G and H, and quantified in I). Although it is believed that alterations in membrane curvature originate from *local* changes in lipid composition, not easily detected through biochemical analysis (Ivanova *et al.*, 2001; Brown *et al.*, 2003), we subjected cells depleted of cPLA2α to analysis of the *total* content of several LPA species (saturated and unsaturated) by liquid chromatography–tandem mass spectrometry (LC-MS/MS; see *Materials and Methods*). LPA is a form of LPL frequently found in biological membranes (Brown *et al.*, 2003), and, indeed, as shown in Figure 1J, all four species decreased as a result of cPLA2α depletion by 4–19%.

Acute manipulation of cPLA2α activity elicits change in tubulation of CD59-containing endosomes

Because cPLA2α depletion, which induced tubulation of CD59-containing endosomes, is a chronic treatment, we next sought to *acutely* manipulate the *activity* of endogenous cPLA2α. This would allow us to relate LPL production in a relevant time scale to endosome maturation events. For this purpose, we pretreated cells for up to 1 h with different PLA2 antagonists and activators and performed a 15-min uptake of CD59 in their presence (Figure 2, A–D; quantified in E). Alternatively, we introduced the reagent only during the 15-min uptake of CD59 (unpublished data). In both time scales the

PLA2 inhibitor methyl arachidonyl fluorophosphonate (MAFP) induced a similar hypertubulation of CD59-containing membranes to that seen upon knockdown of cPLA2α (Figure 2B). However, MAFP can potentially inhibit Ca^{2+}-independent (iPLA2) and Ca^{2+}-dependent (cPLA2) PLA2. Therefore we aimed to reduce free cytosolic calcium levels to prevent recruitment of cPLA2α onto membranes, without affecting iPLA2, by using the chelator 1,2-bis(*o*-aminophenoxy)ethane-*N*,*N*,*N*′,*N*′-tetraacetic acid (BAPTA-AM; Grimmer *et al.*, 2005). As shown in Figure 2C, BAPTA-AM treatment of 1 h or 15 min (unpublished data) during CD59 uptake similarly enhanced tubulation of CD59-containing membranes, rendering a long and elaborate network of tubular membranes (Figure 2C). On the other hand, treatment of cells with melittin, a PLA2 activator peptide, led to exacerbated vesiculation of CD59-containing endosomes with little or no remaining CD59-containing tubules observed after 30 min of treatment (Figure 2D). Tubule formation in these acute treatments was measured by scoring cells with tubule-localized CD59 upon two short treatments with these inhibitors: 15 and 30 min (graph in Figure 2E; see *Materials and Methods*). Although changes in tubulation were evident soon after 15 min with all three reagents compared with untreated cells (Figure 2E, left bars), a more robust change was obtained after 30 min (Figure 2E, right bars), with a sharp decrease in tubulation upon melittin treatment and a twofold increase with MAFP or BAPTA-AM.

Taken together, these acute manipulations of cPLA2α function are in line with the time scale of endosomal-tubule formation during the movement of endocytosed CD59 throughout the endocytic pathway and support our observations with PLA2α siRNA.

cPLA2α associates with CD59-containing endosomes

In the absence of a specific anti-cPLA2α antibody for immunofluorescence applications, we sought to visualize this enzyme in association with CD59-containing endosomes using HA-cPLA2α. Because a large portion of cPLA2α (endogenous or overexpressed) is cytosolic, we used a cytosol washout by perforating the plasma membrane to remove the cytosolic cPLA2α potentially masking a membrane-bound pool. Figure 2F reveals a partial localization of membrane-bound cPLA2α with CD59 endosomes after 15 min of uptake.

Cholesterol-enriched endosomes are affected by cPLA2α knockdown

GPI-APs maintain their association with cholesterol-rich rafts throughout the endocytic pathway (Mayor *et al.*, 1998). We therefore hypothesized that cPLA2α depletion might have a general effect on cholesterol-containing endosomal membranes. To directly address this, we knocked down cPLA2α and used filipin, an autofluorescent polyene macrolide that strongly binds to membrane-embedded cholesterol, to visualize cholesterol-containing membranes. As shown in Figure 2, G and H, hypertubulation of cholesterol-containing membranes was visible, resembling the phenotype observed for internalized CD59. This raised the notion that a more general hypertubulation of endosomes containing cholesterol occurs upon depletion of cPLA2α. Because cholesterol is not considered to be a major component of the clathrin-dependent endocytic pathway, it was not surprising that the distribution of internalized transferrin into endosomes remained mostly unaffected by cPLA2α depletion (Figure 2, I and J), whereas major histocompatibility complex class I (MHC I), which internalizes independent of clathrin (Radhakrishna and Donaldson, 1997) in a cholesterol-dependent manner (Naslavsky *et al.*, 2004), displayed hypertubulation reminiscent of that observed for CD59 and filipin, although to a lesser extent (Figure 2, K and L). To determine whether cPLA2α affects other endocytic organelles in addition to GPI-AP–containing membranes, we monitored early endosomal markers in cells depleted of cPLA2α. Both Rab5 (Supplemental Figure S1, A and B) and EEA1 (Supplemental Figure S1, C and D) displayed moderately enhanced tubulation patterns in the absence of cPLA2α. These data suggest a role for cPLA2α in the fission of cholesterol-containing endocytic tubular membranes.

CD59 tubulation is sensitive to actin dynamics

In our attempt to further characterize CD59 tubular endosomes, we examined the relationship between actin dynamics and the morphology of CD59-containing endosomes. To block depolymerization of the actin filaments, cells were treated first with jasplakinolide, a permeable blocker of actin depolymerization, during which CD59 uptake was allowed. As previously reported by others, numerous cells acquired elongated endosomes that contained CD59 (Supplemental Figure S2B; Shin *et al.*, 2008). Likewise, disrupting the actin filaments with cytochalasin D for 30 min had a similar effect on tubulating CD59-containing endosomes, rendering numerous tubular structures in most cells (Supplemental Figure S2B), similar to earlier reports (Radhakrishna and Donaldson, 1997; Shin *et al.*, 2008). These results indicate that perturbation of actin dynamics can result in membrane tubulation.

cPLA2α promotes vesiculation of EHD1- and MICAL-L1–decorated tubular endosomes

We previously showed that EHD1 partially costains with internalized CD59 on vesicular and tubular endosomes (Cai *et al.*, 2011), but localization of EHD1 to a wider array of membrane tubules was already described (Caplan *et al.*, 2002). Accordingly, we then asked whether endogenous EHD1-decorated endosomes would be affected by the depletion of cPLA2α. Whereas endogenous EHD1 is normally distributed on both tubular and vesicular membranes as well as within the cytoplasm (Figure 3A), upon cPLA2α depletion, there was a considerably greater proportion of endogenous EHD1 localized to tubular membranes (Figure 3B). Reintroduction of a siRNA-resistant HA-cPLA2α cDNA construct into cPLA2α–depleted cells reversed the EHD1 hypertubulation (Figure 3, C and D), indicating that this phenotype indeed results from cPLA2α knockdown.

Because MICAL-L1 was identified as an EHD1 interaction partner that recruits the latter to tubular membranes (Sharma *et al.*, 2009a, 2009b), we performed similar experiments addressing the affect of cPLA2α on endogenous MICAL-L1 localization. As demonstrated, cPLA2α-depletion induced massive hypertubulation of endogenous MICAL-L1 (Figure 3, compare F to E; saturated signal is seen in pseudo-red). Moreover, as we showed for internalized CD59, when cPLA2α was inhibited by MAFP, this also led to increased association of MICAL-L1 with membrane tubules (Figure 3, compare H with G).

Inhibition of lysophospholipid acyltransferase elicits intense vesiculation and disappearance of tubular endosomes

Implicating cPLA2α in the vesiculation of GPI-AP–containing tubular endosomes, we now hypothesized that this might occur through a local accumulation of LPL that promotes membrane curvature formation (a "bottleneck"), thus facilitating subsequent scission of the membranes. Because LPL (mostly LPA) can be further metabolized into phospholipid (PL) by lysophospholipid acyltransferase (LPAT) activity, we sought to induce local accumulation of LPL by inhibiting LPAT activity with CI-976, an inhibitor of acylCoA cholesterol acyltransferase that effectively inhibited a Golgi-associated LPAT (Harte *et al.*, 1995; Drecktrah *et al.*, 2003). This treatment completely disrupted CD59-containing tubules (akin to the melittin treatment),

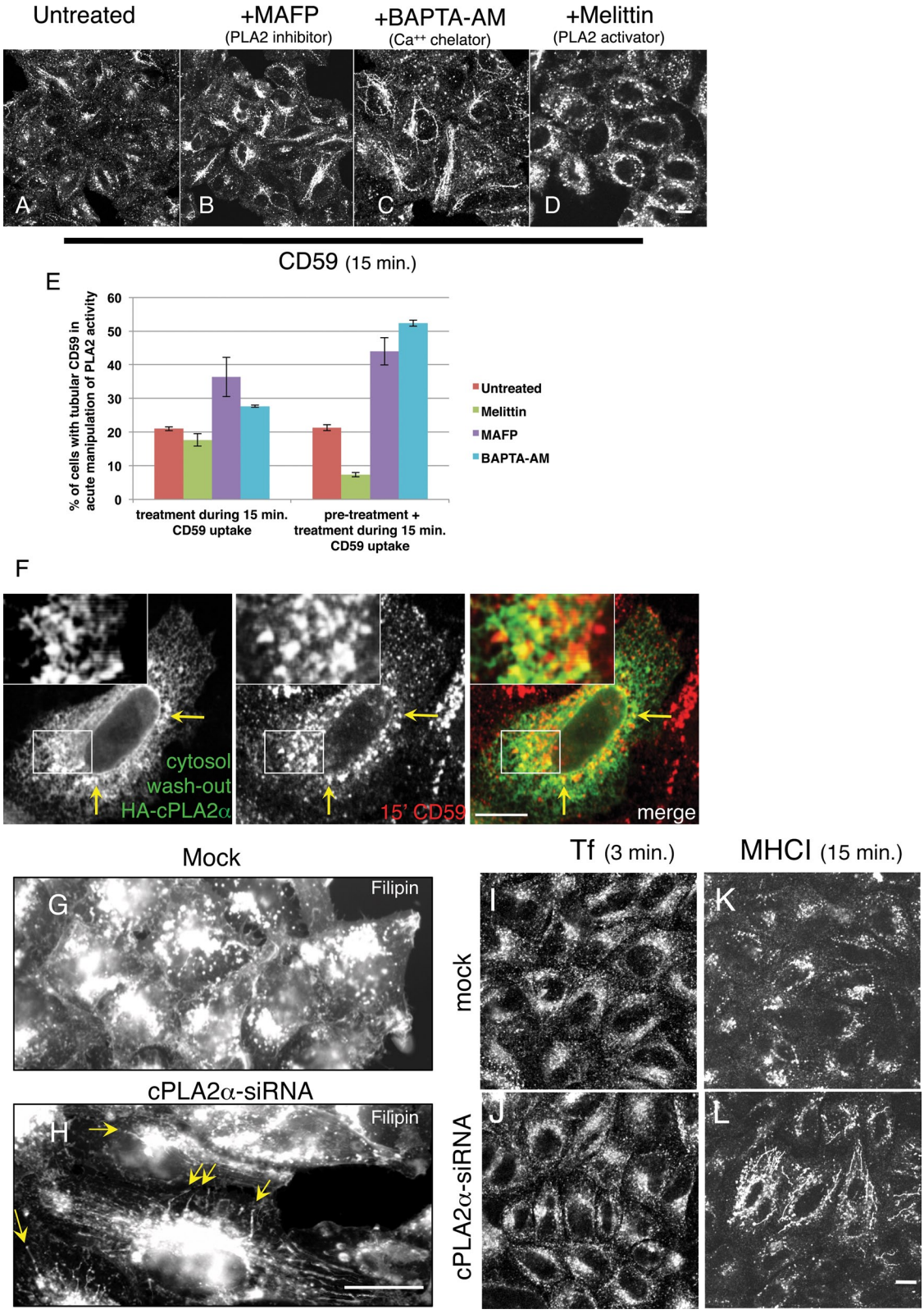

FIGURE 2: Acute manipulation of cPLA2α affects vesiculation of CD59-containing endosomes. (A–D) HeLa cells growing on coverslips were either untreated (A) or pretreated with either PLA2 inhibitor MAFP (65 μM; B) or calcium chelator BAPTA-AM (50 μM; C) for 1 h or PLA2 activator melittin (2 μM; D) for 30 min. The pretreated cells were then incubated with anti-CD59 antibody for 15 min in the presence of the corresponding pharmacological agents, followed by acid stripping, fixation, and incubation with Alexa 568–conjugated anti-mouse antibody. (E) Quantification of the percentage of cells with tubular CD59 upon the treatment of pharmacological agents was done from three experiments: Cells were pulsed with anti-CD59 antibody in the presence of pharmacological agents for 15 min either with no pretreatment or pretreatment with melittin for 10 min and with MAFP or BAPTA-AM for 20 min. SE is shown. (F) Cells growing on

giving way to vesicles partially decorated by GFP-myc-EHD1, which normally associates with tubules (Figure 3, compare J to I). Taken together, these data further link LPL with scission/vesiculation of GPI-AP–containing endosomes.

How does cPLA2α affect endocytic trafficking?

Because cells treated with cPLA2α-siRNA caused endosomal tubulation at various time points (3–30 min), we hypothesized that cPLA2α might affect endosomes at different phases of maturation, including deep plasma membrane invaginations (see Figure 1, B and C), as well as sorting and recycling endosomes. Since cPLA2α affected a more general population of cholesterol-containing endosomes, we opted to methodically measure *endocytosis* and *recycling* of cargoes internalized via three different pathways (clathrin-dependent and clathrin-independent, as well as raft-associated uptake) while manipulating cPLA2α activity. To do so, we took advantage of the Tac construct chimeras (the α subunit of interleukin-2), which have modified C-termini: the wild-type Tac enters cells in a clathrin-independent manner (Radhakrishna and Donaldson, 1997; Lamaze *et al.*, 2001), whereas Tac-GPI chimera possesses the GPI moiety that targets it to rafts and caveolae (Delahunty *et al.*, 1993). Tac-LL is a chimera composed of the extracellular, lumenal, and transmembrane domains of Tac and the cytoplasmic tail of the mouse CD3 γ chain containing a DKQTLL motif that directs this molecule to bind to clathrin-related adapters (Delahunty *et al.*, 1993; Corvera *et al.*, 1994).

Using the same antibody (anti-Tac) for the three transfected cargoes, we monitored their *internalization* for up to 1 h and found that all three cargoes internalized at modestly increased rates (by 12–15%) upon cPLA2α depletion (Figure 4A). A similar increase was also recorded for endogenous CD59 (unpublished data). We further measured the internalization rate of the three cargoes under acute manipulation of cPLA2α activity (Figure 4B) with PLA2 inhibitors and an activator that had earlier induced changes in the tubulation patterns of CD59-containing endosomes (see Figure 2). Although this pharmacological approach may have a broader and less specific effect on cPLA2α, it nevertheless induces acute change in cPLA2α activity, as opposed to the chronic depletion of the enzyme upon siRNA treatment. A 30-min pretreatment with the cPLA2α activator melittin (Figure 4B) decreased the endocytic rate of all three cargoes by varying degrees (13–49%). This is in line with the moderate *increase* seen upon cPLA2α depletion for all three cargoes (compare to Figure 4A). The inhibitor MAFP had little influence on the internalization rate of the cargoes, whereas the chelator BAPTA-AM (Figure 4B), which dramatically decreased their internalization (by 47–64%), may affect multiple calcium-dependent enzymes involved in endocytosis. Together these quantitative data lead us to suggest that cPLA2α plays a modest and/or dispensable role in the regulation of proteins internalizing by distinct modes of endocytosis.

Knocking down cPLA2α affected EHD1- and MICAL-L1–decorated endosomes (Figure 3). Because both EHD1 and MICAL-L1 are primarily regulators of recycling endosomes, we aimed to assess the involvement of cPLA2α in the return of internalized cargo back to the plasma membrane. To this aim, we again transfected Tac chimeras. The extent of the cargo recycling to the cell surface was measured by anti-Tac reappearing at the plasma membrane. As seen in Figure 4C, Tac-GPI, which under mock conditions recycled 52% of its internalized pool within 2 h, displayed slightly decreased recycling (46%) upon siRNA-cPLA2α treatment. Likewise, CD59 recycling had a similar mild response to cPLA2α knockdown (unpublished data). Of interest, of the three recycling cargoes, Tac-GPI was the most affected by this treatment. On acute manipulation of cPLA2α, the three cargoes continued to show a common trend, as observed for internalization (Figure 4D): MAFP and BAPTA-AM partially slowed recycling, with Tac-GPI again being the most affected. On the other hand, melittin had little effect on recycling. Connecting these measurements with the morphology seen for CD59-containing endosomes (in Figures 1 and 2) shows that hypertubulation partially alters transport of vesicles containing cargo.

Overexpression of cPLA2α does not alter endosome tubulation

Because both depletion and inhibition of cPLA2α caused enhanced localization of internalized CD59 to tubular membranes, and because activation of cPLA2α apparently increased vesiculation of CD59-containing endosomes, we hypothesized that overexpression of the enzyme might promote scission of tubular endosomes. Accordingly, we transfected HA-cPLA2α into HeLa cells and monitored the distribution of internalized CD59 (Supplemental Figure S3, A and B). Surprisingly, the HA-cPLA2α–overexpressing cells (yellow border in A, green cells in B) exhibited a similar degree of tubule-associated CD59 as the nontransfected cells. More broadly, HA-cPLA2α overexpression did not decrease the association of endogenous MICAL-L1 with tubular membranes (Supplemental Figure S3, C and D; HA-cPLA2α-transfected cells in yellow borders). These data suggest that whereas cPLA2α may promote vesiculation, additional proteins and/or modes of activation are likely required.

EHD1, but not dynamin II, cooperates with cPLA2α in the course of vesiculation

We next used a candidate-based approach to search for additional proteins involved in the scission process of GPI-AP–containing tubular membranes, in concert with cPLA2α. Dynamin II has a well-documented role in the scission of clathrin-coated pits (van der Bliek *et al.*, 1993; Damke *et al.*, 1994) and the Golgi stacks (Grimmer *et al.*, 2005; Kessels *et al.*, 2006; Jaiswal *et al.*, 2009). Using an inhibitor, dynamin was also found to participate in endosome fission (Mesaki *et al.*, 2011). However, GPI-APs and other raft-residing cargoes do not require dynamin II for their internalization (Sabharanjak *et al.*, 2002). Accordingly, we asked whether involvement of dynamin II at a postinternalization stage might have an affect on shaping

coverslips were transfected with HA-cPLA2α. After 16 h, cells were pulsed with mouse anti-CD59 antibody for 15 min at 37°C and acid stripped, followed by cytosol washout in PBS containing 0.05% saponin and 0.1% BSA for 30 s. After fixation, cells were stained with rabbit anti-HA antibody for 1 h, followed by Alexa 568–conjugated anti-mouse and Alexa 488–conjugated anti-rabbit antibodies. Yellow arrows in F show the colocalization of HA-cPLA2α with internalized CD59. cPLA2α affects cholesterol-containing endosomes. (G–L) Cells were mock treated (G, I, K) or treated with cPLA2α-siRNA (H, J, L). For cholesterol staining (G, H), fixed cells were quenched in 50 mM NH_4Cl for 10 min and incubated with 1 mg/ml filipin for 30 min. Yellow arrows in H indicate hypertubulation detected by filipin. For transferrin uptake (I, J), HeLa cells were starved in serum-free DMEM media (containing 0.5% BSA) for 30 min and then incubated with Alexa 568–conjugated transferrin for 3 min, followed by fixation. (K–L) Cells were incubated with anti-MHC I antibody for 15 min at 37°C, acid stripped, and fixed. Internalized MHC I was detected with Alexa 568–conjugated anti-mouse antibody. Bar, 10 μm.

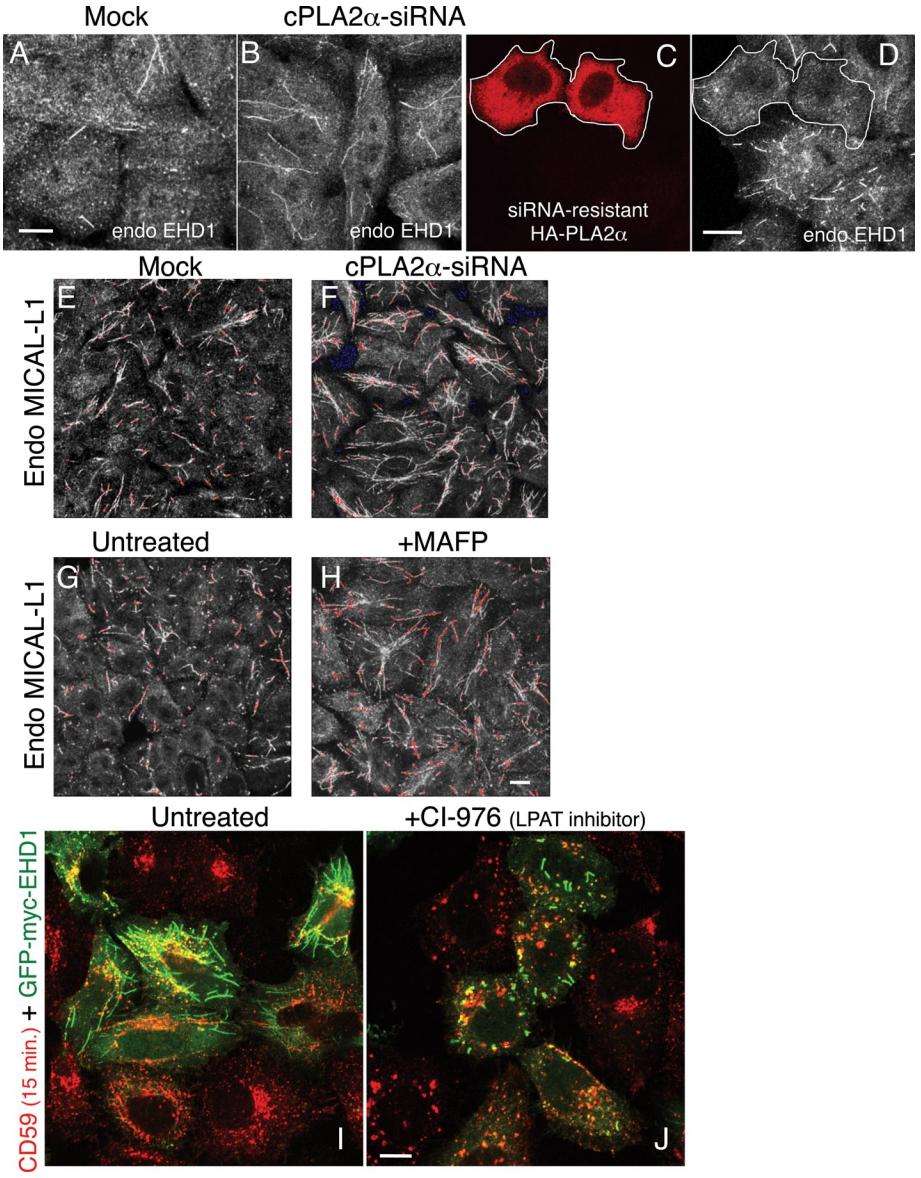

FIGURE 3: Depletion of cPLA2α induces hypertubulation of EHD1- and MICAL-L1–decorated membranes, whereas inhibition of LPAT induces vesiculation of EHD1-containing membranes. (A–F) HeLa cells growing on coverslips were mock treated (A, E) or treated with cPLA2α–siRNA (B– D, F) for 48 h and fixed. Cells were then stained with anti-EHD1 antibody, followed by Alexa 568–conjugated anti-rabbit antibody (A, B). For rescue experiments, siRNA-resistant HA-cPLA2α was transfected into cPLA2α-depleted cells (C, D) and costained with anti-HA and anti-EHD1 antibodies. The white border denotes transfected cells. (E, F) Cells were stained with mouse anti-MICAL-L1 antibody, followed by Alexa 568–conjugated anti-mouse antibody. (G, H) Cells were either left untreated (G) or pretreated with 65 μM MAFP (H) for 1 h. Cells were then fixed and stained with anti–MICAL-L1 antibodies. Saturated signal captured in images E–H are shown in pseudo red. (I, J) Cells were transfected with GFP-myc-EHD1. After 16 h, cells were either untreated (I) or pretreated with 80 μM CI-976 (J) for 1 h. Both untreated and pretreated cells were then pulsed with anti-CD59 antibody for 15 min in the absence (I) or presence of CI-976 (J), followed by acid stripping, fixation, and incubation with Alexa 568–conjugated anti-mouse antibody. Bar, 10 μm.

GPI-AP–containing membranes. To this aim, we transfected a dominant-negative dynamin II mutant (K44A) into HeLa cells. We first validated the efficacy of this mutant in our system, showing that internalization of transferrin was severely impaired in transfected cells (Figure 5, A and B, compare transfected cells in green [A] or within the white borders [B] to neighboring cells). However, since dynamin does not affect internalization of clathrin-independent receptors (such as CD59), we reasoned that if dynamin II (K44A) prevents scission of GPI-AP–containing tubular membranes, we would expect to observe increased levels of tubular structures containing internalized CD59. However, this mutant had no discernible effect on CD59-containing tubules (Figure 5, C and D; transfected cells are in green and are highlighted by the white border). These observations suggest that dynamin II is not a major facilitator of vesiculation of GPI-AP–containing tubular endosomes. Other proteins that have recently been implicated as "pinchases" of endocytic membranes are EHD2 (Daumke *et al.*, 2007) and EHD1 (Jakobsson *et al.*, 2011). To test the potential role of EHD1 in GPI-AP–containing tubular membrane scission, we depleted cells of endogenous EHD1 by siRNA (Figure 5E). Greater than 90% loss of EHD1 expression induced two apparent alterations: 1) a massive relocation of internalized CD59 to the perinuclear endocytic recycling compartment, denoted in Figure 5G by asterisks, consistent with our previous findings (Cai *et al.*, 2011), and 2) a significant increase of tubular membranes containing internalized CD59 (Figure 5; compare G to F and see insets). Therefore we propose a role for EHD1 in scission of GPI-AP–containing tubules.

cPLA2α interacts with EHD1

We next hypothesized that cPLA2α and EHD1 might function as a complex to regulate GPI-AP tubule scission. We first sought to determine whether EHD1 and cPLA2α could be detected on mutual membrane structures in vivo. As described in Figure 2, we were limited by the cytoplasmic localization of cPLA2α. To overcome this technical problem, which may mask association with membranes, we used a proximity assay, which detects whether two proteins are localized within ~40 nm of each other (Soderberg *et al.*, 2006). We first demonstrated that GFP-myc-EHD1 and HA-cPLA2α were coexpressed in almost all transfected cells (Figure 6A), as were MICAL-L1 and EHD1, which served as the positive control pair (Figure 6B), and JNK1 and EHD1, which served as the negative control pair (Figure 6C). Quantification indicated that all three pairs showed >95% coexpression (unpublished data). In cells coexpressing EHD1 and cPLA2α (Figure 6D; see green border area; nuclei are shown in blue) red dots were easily detected, each representing a single proximity event (quantified in Figure 6G). For the positive control, MICAL-L1 and EHD1 showed a large number of proximity events, as expected (Figure 6E and quantified in G). On the other hand, despite high levels of expression, JNK1 and EHD1 displayed almost no proximity

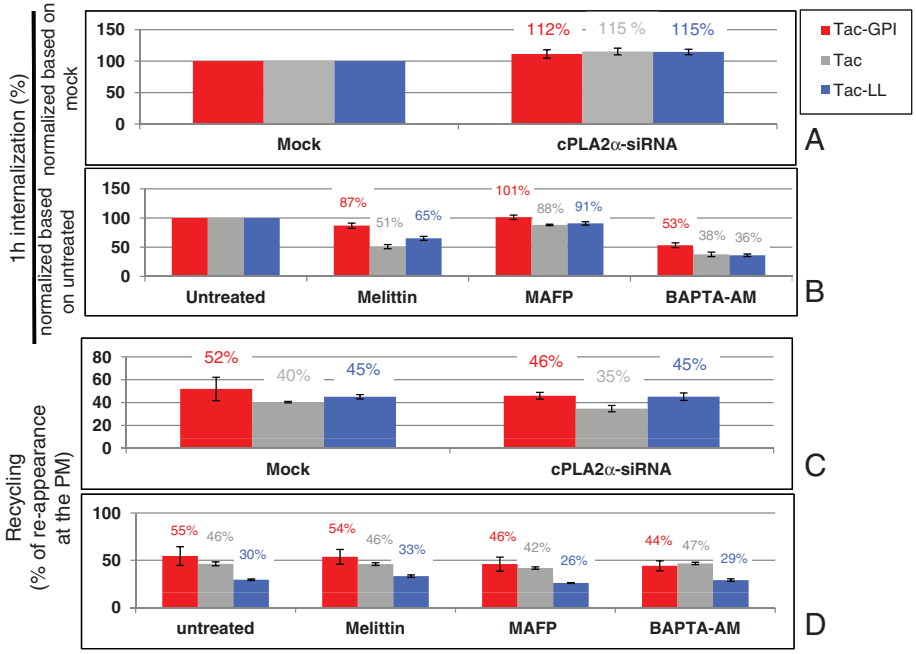

FIGURE 4: cPLA2α activity modestly affects cargoes trafficking through different endocytic pathways. (A–D) The effect of cPLA2α-siRNA and pharmacological agents on the trafficking of Tac-GPI, Tac, and Tac-LL was studied. (A) For the effect of cPLA2α-siRNA on the internalization of cargoes, Tac-GPI, Tac, and Tac-LL were transfected respectively into either mock-treated or cPLA2α-siRNA–treated cells. Cells were then pulsed with mouse anti-Tac antibody for 1 h. After acid stripping and fixation, cells were incubated with Alexa 647 goat anti–mouse F(ab)2 antibody in the presence of saponin. (B) For the effect of pharmacological agents on the internalization of cargoes, cells were untreated or pretreated for 30 min with 2 μM melittin or for 1 h with 65 μM MAFP or 50 μM BAPTA-AM. Cells were then pulsed with anti-Tac antibody for 1 h in the presence of corresponding agents, followed by acid stripping. After fixation, cells were stained with Alexa 647 goat anti–mouse F(ab)2 antibody in the presence of saponin. (C) For the effect of cPLA2α-siRNA on the recycling of cargoes to the PM, after either mock or siRNA treatment, cells were pulsed with anti-Tac antibody for 1 h, stripped, and chased in complete media for 2 h, followed by fixation. (D) For the effect of pharmacological agents on the recycling of cargoes to the PM, cells were pulsed with anti-Tac for 1 h and stripped. Cells were then chased in complete media with different pharmacological agents for 2 h, followed by fixation. Internalized Tac was measured with Alexa 647–conjugated anti–mouse F(ab)2 antibody in the presence of saponin, whereas detection of Tac reappearing at the surface was assessed in the absence of saponin. Percentage of recycling was calculated as a ratio of the reappearing Tac/internalized Tac. Measurements were carried out by flow cytometry analyses of three independent experiments for each plot. Error bars indicate SE.

events (Figure 6F and quantified in G). These data indicate that EHD1 and a portion of cPLA2α are proximally localized in vivo.

To determine whether EHD1 and cPLA2α are found in the same complex, we performed coimmunoprecipitation studies. Either HA-cPLA2α or HA-JNK1 (negative control) were transfected into HeLa cells. After lysis, HA-cPLA2α (Figure 6H, lane 1) or HA-JNK1 (Figure 6H, lane 2) could be detected by immunoblot. Similar levels of endogenous EHD1 were also detected in both sets of transfected cell lysates (Figure 6H, lanes 1 and 2). When the two sets of lysates were immunoprecipitated with anti-EHD1 antibody, a band corresponding to HA-cPLA2α was readily detected (Figure 6H, lane 3, red arrow), whereas the negative control protein, HA-JNK1, could not be observed (Figure 6H, lane 4). Taken together, these data suggest that cooperation between cPLA2α and EHD1 likely occurs in a complex.

Although EHD1 and cPLA2α reside in part on the same complex as judged by their coimmunoprecipitation, we were unsuccessful in showing their interaction by selective yeast two-hybrid assays (Figure 6I), although a positive interaction between EHD1 and MICAL-L1 was observed. These data support the notion that EHD1 and PLA2α interact in an indirect manner.

cPLA2α–EHD1 scission complex

The ability of EHD proteins to perform tubule scission was postulated by others (Daumke *et al.*, 2007). However, overexpressing EHD1 in vivo is insufficient to catalyze this process; overexpressed EHD1 extensively decorates existing tubular structures, and this remains unchanged even when cPLA2α is highly coexpressed (unpublished data). This hints at a complex consisting of multiple components, beyond cPLA2α and EHD1. To further connect EHD1-scission activity with GPI-AP tubular endosomes, we took advantage of a truncated EHD1 protein lacking its C-terminal EH domain (ΔEH), which no longer resides on tubular membranes. This mutant localizes exclusively to vesicular structures (Caplan *et al.*, 2002), raising the possibility that the EH domain might serve as a regulatory region that slows down unmitigated scission. We therefore asked whether tubular GPI-AP endosomes can be vesiculated by expression of the apparent highly efficient "vesiculator" EHD1(ΔEH). To test this idea, hypertubulation of GPI-AP endosomes was induced by cPLA2α-siRNA, with subsequent internalization of CD59 into cells expressing EHD1(ΔEH). As demonstrated (Figure 7A), in untransfected cells, CD59 localized to an array of hypertubular endosomes. However, cells expressing GFP-myc-EHD1(ΔEH) displayed a dramatic shift of CD59 from tubules to vesicles (Figure 7A and B; see transfected cells in yellow-bordered region). Moreover, overexpression of the GFP-myc-EHD1(ΔEH) mutant had a similar affect on the endogenous MICAL-L1 and reduced its localization to membrane tubules (Figure 7, C and D; see yellow-bordered region). Overall, these data support a role for cPLA2α and EHD1 in the regulation of membrane scission for tubules containing GPI-APs.

DISCUSSION

Studies in recent years have established a wide range of cellular participants engaged in remodeling membranes, using both protein- and lipid-based mechanisms (reviewed in Prinz and Hinshaw, 2009; Campelo *et al.*, 2010; Graham and Kozlov, 2010; Hurley, 2010). Our results implicate cPLA2α in the vesiculation of GPI-AP–containing tubular endosomes, possibly through a local accumulation of LPL catalyzed by cPLA2α (see model, Figure 8). The LPL accumulation may promote membrane curvature by forming a "bottleneck," thus preparing the membranes for subsequent scission. We demonstrate here that both depletion of cPLA2α and its inhibition give rise to long and abundant tubular endosomes, whereas its activation brings about a substantial vesiculation of

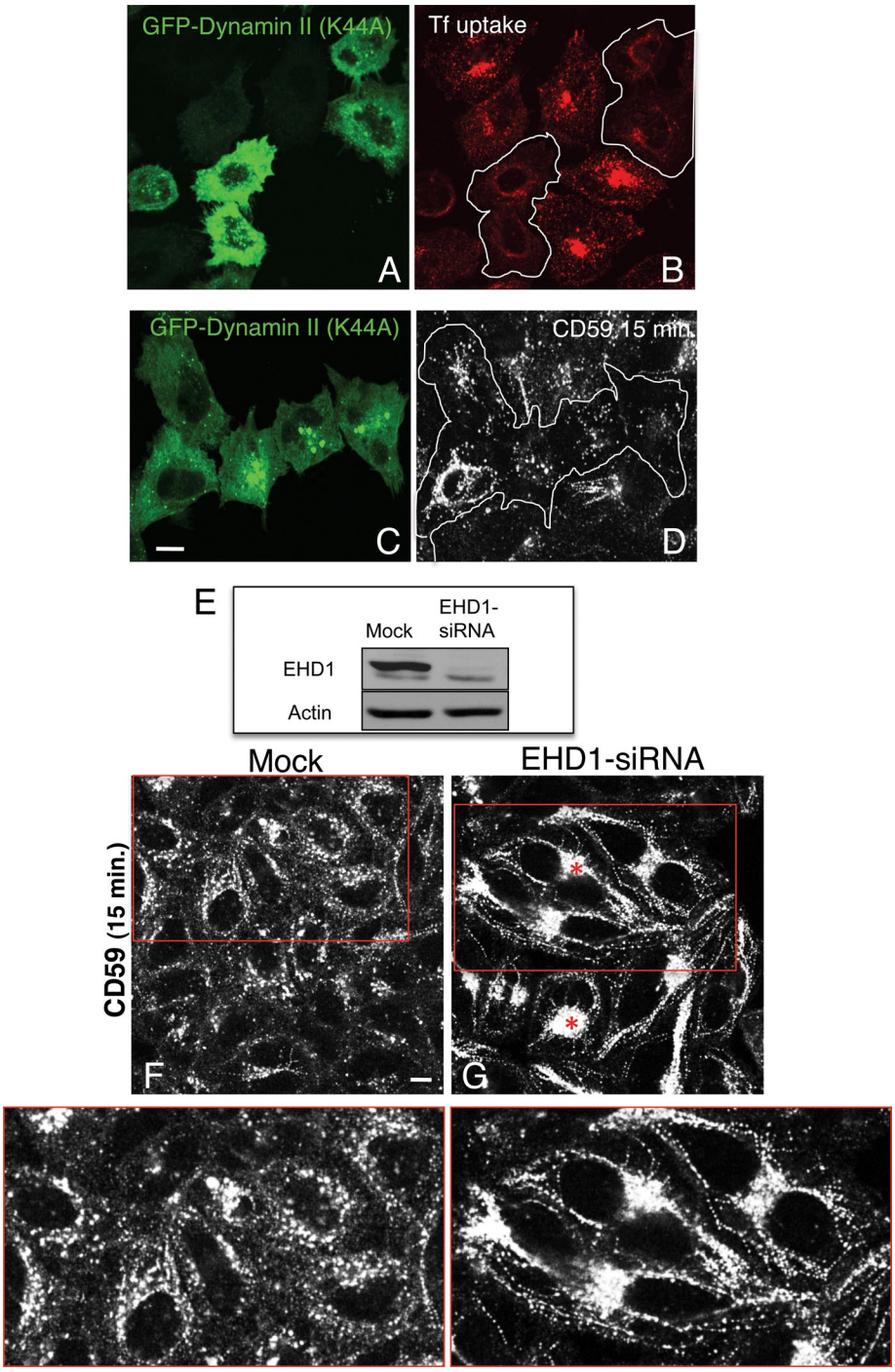

FIGURE 5: EHD1, but not dynamin II, participates in the vesiculation of CD59 tubular endosomes. (A–D) HeLa cells growing on coverslips were transfected with the GFP-dynamin II dominant-negative mutant (K44A) for 16 h. Transfected cells are denoted by a white border in B and D. Cells were either incubated with Alexa 568–conjugated transferrin for 10 min and fixed (A, B) or pulsed with anti-CD59 antibody for 15 min at 37°C (C, D). After acid stripping (C, D), cells were fixed and stained with Alexa 568–conjugated anti-mouse antibody. (E) HeLa cells growing in 35-mm dishes were either mock treated or treated with EHD1-siRNA for 48 h. Cells were lysed, and proteins were separated by SDS–PAGE and immunoblotted with antibodies against EHD1 (top) and actin (bottom; loading control). (F, G) HeLa cells growing on coverslips were mock treated (F) or treated with EHD1-siRNA (G). After 48 h, cells were pulsed with anti-CD59 antibody for 15 min at 37°C, stripped, fixed, and then stained with Alexa 568–conjugated anti-mouse antibody. Red boxed areas are shown in higher magnification. Asterisks denote the endocytic recycling compartment. Bar, 10 μm.

these endosomes. Owing to its inverted-cone–shaped structure, LPA found in membranes could be a major lipid contributor to their high-curvature outline. Measurement of total cellular LPA content (of different acyl length) in cPLA2α-depleted cells could be indicative of a broader change in LPL under these conditions. A decrease of 4–19% in the total LPA in this study may mean that *local* change in LPA levels may be greater, although this is difficult to monitor (Brown *et al.*, 2003). Accordingly, inhibition of LPAT activity caused massive vesiculation, possibly through the accumulation of local LPL, further linking this lipid with efficient vesiculation of GPI-AP endosomes (Figure 8). Of importance, even short-term drug treatments targeting cPLA2α activity were enough to alter the morphology of CD59-containing endosomes (Figure 2E), suggesting a putative role for the enzyme on a time scale relevant to endosome formation and maturation.

On the basis of the indirect interaction between EHD1 and cPLA2α and the hypertubulation observed under EHD1-siRNA treatment, we further propose that EHD1 cooperates with cPLA2α to promote completion of the vesiculation process. Observing that a wide population of endosomes is affected by cPLA2α (determined by staining for cholesterol-MICAL-L1-EHD1 as well as early endosomes), we quantitatively recorded the impact of hypertubulation on the general transport of endosomes throughout the endocytic pathway by flow cytometry. Tac-GPI, Tac, and Tac-LL were ideal cargoes to conduct a comparative study of three described endocytic pathways. cPLA2α knockdown modestly altered trafficking of GPI-AP (Tac-GPI and CD59), as well as cargo internalizing independent of rafts (Tac-LL): the rate of internalization for all three Tac cargoes was slightly enhanced to a similar extent (12–15%), a finding that may be related to previous reports showing cPLA2 binding to caveolin1 in mouse hippocampal neuron cultured cells (Gaudreault *et al.*, 2004) and to phosphatidylinositol (4,5)-bisphosphate (Casas *et al.*, 2006). On a shorter time scale, perturbation of cPLA2α activity with different drugs had a somewhat greater influence on endocytosis of all three cargoes, reducing their internalization compared with untreated cells or cPLA2α-knockdown cells. This indicates that a fine balance of cPLA2α activity may be needed for endocytosis, in both membrane shaping and signal transduction.

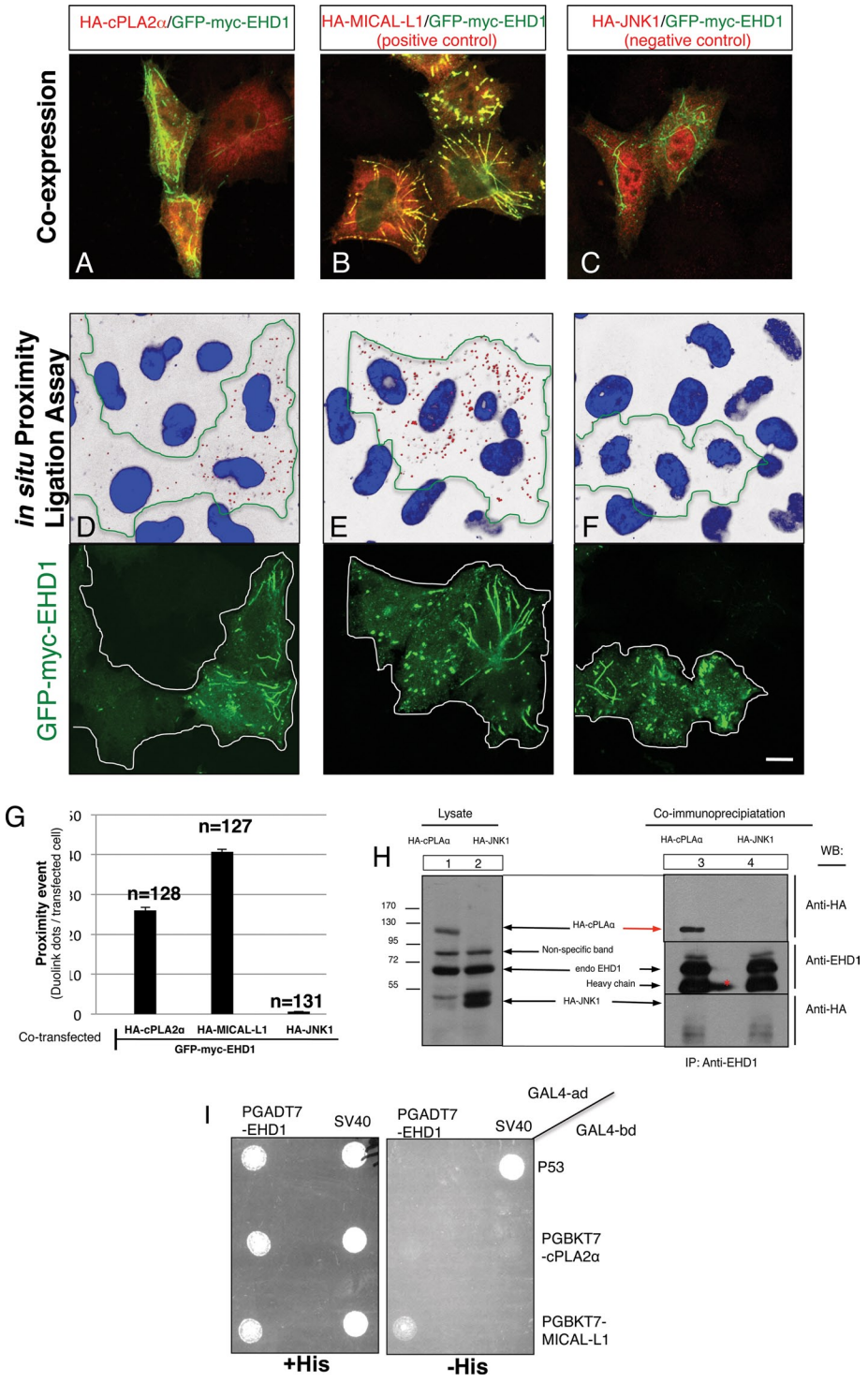

FIGURE 6: cPLA2α and EHD1 are proximally localized and interact in vivo. (A–F) HeLa cells growing on coverslips were cotransfected with GFP-myc-EHD1 and HA-cPLA2α (A, D), HA-MICAL-L1 (positive control; B, E), or HA-JNK1 (negative control; C, F) for 16 h. Coexpression for each pair was evaluated in A–C by staining one set of cells with mouse anti-HA antibody, followed by appropriate secondary antibody. A double stain (mouse anti-HA and rabbit anti-myc antibody) was performed for the proximity assay (D–F; see *Materials and Methods*). Each red dot detected is a single proximity event between anti-myc and anti-HA antibodies (transfected cells, identified with GFP, are marked with green lines; D–F). (G) Quantification of the number of red dots per transfected cell was done using data from three independent experiments. (H) HeLa cells were grown in 100-mm dishes and transfected with either HA-cPLA2α or HA-JNK1 (negative control). After 20 h, cells were lysed for 1 h in buffer containing 50 mM Tris, pH 7.4, 150 mM NaCl, 0.5% Brij 98, and protease inhibitors. For pull-down, cell lysates were incubated with rabbit anti-EHD1 antibody overnight. Rabbit IP Matrix beads were added to the mixture of cell lysate and EHD1 antibody for 3 h at 4°C. Beads were washed in buffer containing 50 mM Tris, pH 7.4, 150 mM NaCl, and 0.1% Brij 98. Proteins were eluted by adding SDS loading buffer. Samples were subjected to 8% SDS–PAGE, followed by blotting with anti-HA antibody. Red arrow in H indicates HA-cPLA2α pulled down by EHD1. Red star denotes spillover of the IgG heavy chain. (I) The *S. cerevisiae* yeast strain AH109 was cotransformed with the indicated GAL4-binding domain (GAL4bd) fusion constructs (including GAL4bd-cPLA2α and GAL4bd-MICAL-L1) and GAL4bd-p53 (control), together with the indicated GAL4 transcription activation (GAL4ad) fusion constructs GAL4ad-EHD1 and GAL4ad-SV40 large T-antigen (control). The cotransformants were assayed for their growth on nonselective (+HIS) and selective (–HIS) media. Bar, 10 μm.

Likewise, a mild effect of hypertubulation on recycling was observed for the three cargoes: on cPLA2α depletion, recycling of Tac-GPI, CD59 (unpublished data), and Tac (both believed to reside within cholesterol-containing endosomes) was moderately delayed, whereas Tac-LL recycling remained unaffected (Figure 4). This delay was more evident for Tac-GPI at short treatments with MAFP and BAPTA-AM, compared with the other two Tac cargoes. Whereas activation of cPLA2α with melittin resulted in vast vesicular distribution of CD59, it did not alter its transport back to the plasma membrane, nor did it do so for the other two Tac cargoes. Although vesicles laden with cargo might conceivably be more easily transported along microtubules to the cell surface compared with cargo associated with tubular membranes, motor proteins may be the limiting step, controlling the rate of vesicles that recycle. We speculate that the modest inhibition observed in recycling under conditions of hypertubulation could result from cargo shunting to an alternative route of recycling (fast recycling), occurring directly from peripheral endosomes partly bypassing the tubular recycling compartment.

Most of the studies addressing the involvement of PLA2 in membrane dynamics have focused on the Golgi membranes (de Figueiredo *et al.*, 2001; Grimmer *et al.*, 2005; San Pietro *et al.*, 2009). The processes of vesiculation and tubulation of the Golgi membranes are maintained in a careful balance. This fine-tuning relies in part on the equilibrium between local formation and accumulation of inverted-cone–shaped lipids versus cylinder-shaped lipids in the membrane leaflets. Multiple enzymes oversee

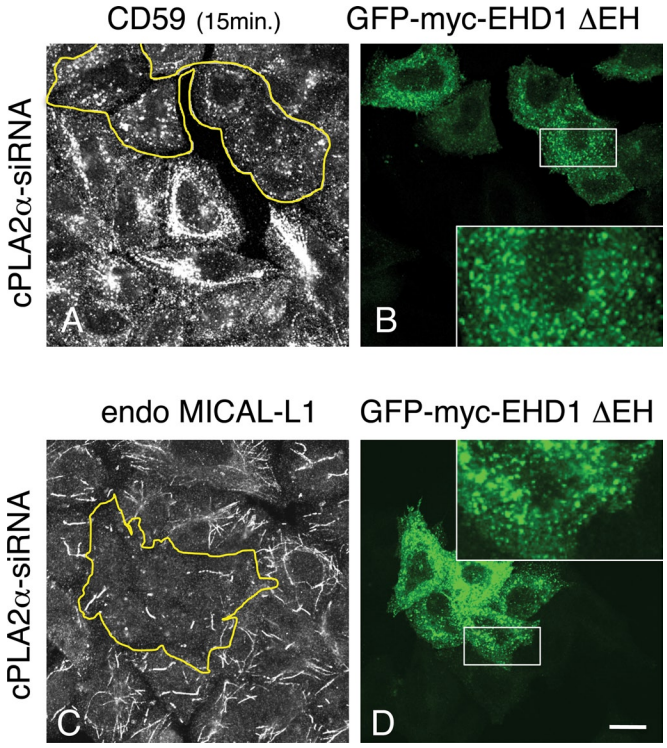

FIGURE 7: The EHD1(ΔEH) mutant vesiculates both CD59- and MICAL-L1–containing tubular endosomes in the absence of cPLA2α. (A–D) cPLA2α-siRNA–treated cells were transfected with the mutant GFP-myc-EHD1(ΔEH). (A, B) After 16 h, cells were incubated with anti-CD59 antibody for 15 min at 37°C, acid stripped, fixed, and stained with Alexa 568–conjugated anti-mouse antibody. (C, D) After transfection, cells were fixed and stained with anti–MICAL-L1 antibody for 1 h, followed by Alexa 568–conjugated anti-mouse antibody. Yellow borders indicate the transfected cells. White boxed areas are shown in higher magnification. Bar, 10 μm.

this equilibrium, as their metabolites directly shape the membranes. A key metabolite of PLA2, LPL, is an inverted-cone–shaped lipid that is generated by hydrolysis of membrane phospholipids and triggers the formation of positive curvature of membrane leaflets at the Golgi. LPL can be further converted into the cone-shaped PL by proteins containing LPAT activity (reviewed in Brown *et al.*, 2003; Kooijman *et al.*, 2003).

The precise role of PLA2 in the Golgi may be very complex. A study by Grimmer *et al.* (2005) demonstrated that cPLA2 is recruited to the Golgi by cholesterol, where it induces the vesiculation of the Golgi stacks. In apparent contrast, an equally compelling study by San Pietro *et al.* (2009) showed that cPLA2α is capable of tubulating the Golgi membranes. In addition, earlier data implicate iPLA2 in the tubulation of Golgi stacks (de Figueiredo *et al.*, 2001) and provide evidence that LPAT activity promotes their vesiculation (Chambers *et al.*, 2005).

The notion of PLA2 enzymes involved in the modulation of early endosomal membranes has been given more attention recently. For example, the catalytic subunits α1 and α2 of PAFAH Ib were found to be an early endosome–associated PLA2, promoting tubule formation and affecting transferrin trafficking (Bechler *et al.*, 2011). Our observations associate cPLA2α with morphological effects on early endosomes (seen with Rab5 and EEA1), as well as on wider populations of vesicles, possibly containing cholesterol.

Despite previous studies, the potential function of cPLA2α in cholesterol-containing endosomes that transport GPI-AP has not been addressed. The use of cPLA2α depletion (chronic treatment) in this study, in combination with short/acute manipulation of the enzyme activity (with inhibitors and an activator), allowed us to derive a function for this enzyme that is largely consistent with its function at the Golgi (Grimmer *et al.*, 2005). Although our study and those of Grimmer *et al.* (2005) suggest that cPLA2α is involved in membrane vesiculation (rather than tubulation), it is likely that the activity of these complex enzymes may have different roles, depending upon the membranes to which they localize and their specific lipid compositions.

Cholesterol has been described as an important factor that modulates membrane susceptibility to cPLA2 (Klapisz *et al.*, 2000; Grimmer *et al.*, 2005). Although Golgi membranes, which contain high levels of cholesterol, were the main organelle studied with respect to cPLA2 modulation, endosomes, and in particular those containing GPI-AP and cholesterol/sphingolipid-rich microdomains, have been largely overlooked. Although one study did provide in vitro evidence for the involvement of PLA2 in vesiculating raft-containing giant liposomes based on a physicochemical mechanism (Staneva *et al.*, 2004), little is known about the role of cPLA2 on GPI-AP–containing membranes in vivo.

Actin was previously described as one of the driving forces in domain formation on endosomes (Puthenveedu *et al.*, 2010). It has been implicated in tubular-membrane scission either alone (Romer *et al.*, 2010) or in synergy with dynamin (Roux *et al.*, 2006). Shin *et al.* (2008) showed enhanced tubulation of membranes upon both polymerization and depolymerization of the actin filaments. Likewise, here we find that CD59-containing endosomes are sensitive to perturbation of actin dynamics, and when these dynamics are impaired, there is delayed scission that gives rise to elongated tubules (Supplemental Figure S2B).

A fine-tuned pace of endosomal vesiculation, including GPI-AP endosomes, is probably attained by the dual (and opposing) activities of cPLA2α and LPAT, controlling the local accumulation and ratio of LPL versus PL, respectively (mostly LPA and PA). This is consistent with the balance described at the Golgi (de Figueiredo *et al.*, 2001; Drecktrah *et al.*, 2003). We propose that by blocking LPAT activity with the inhibitor CI-976, LPL fails to become further acylated and instead accumulates locally to induce the generation of highly curved buds that culminate in intense vesiculation. This provides a potential molecular explanation for cPLA2α-driven vesiculation of GPI-AP endosomes.

The general involvement of cPLA2α in the vesiculation of cholesterol-containing endosomal structures is evident from our cPLA2α-knockdown treatment followed by filipin staining (Figure 2, G and H), MICAL-L1 staining (Figure 3, E and F), MHC I uptake experiments (Figure 2, K and L), and visualization of early endosomal markers (Supplemental Figure S1). These data illustrate that a wide array of endosomal populations, ranging from incoming clathrin-independent-pathway vesicles to early endosomes and recycling endosomes, similarly display hypertubulation when cPLA2α is absent.

We propose that endosome-bound cPLA2α forms part of a "scission complex," likely with multiple components. Here we describe and visualize two such components: cPLA2α and EHD1. On depletion of either of these proteins, scission was impaired. Reintroduction of the siRNA-resistant cPLA2α in cells treated with cPLA2α-siRNA restored the "scission complex" activity, returning vesiculation to its normal rate (Figure 1, E and F). On the other hand, overexpression of only cPLA2α or EHD1 (or both simultaneously; our unpublished data) did not culminate in enhanced vesiculation of

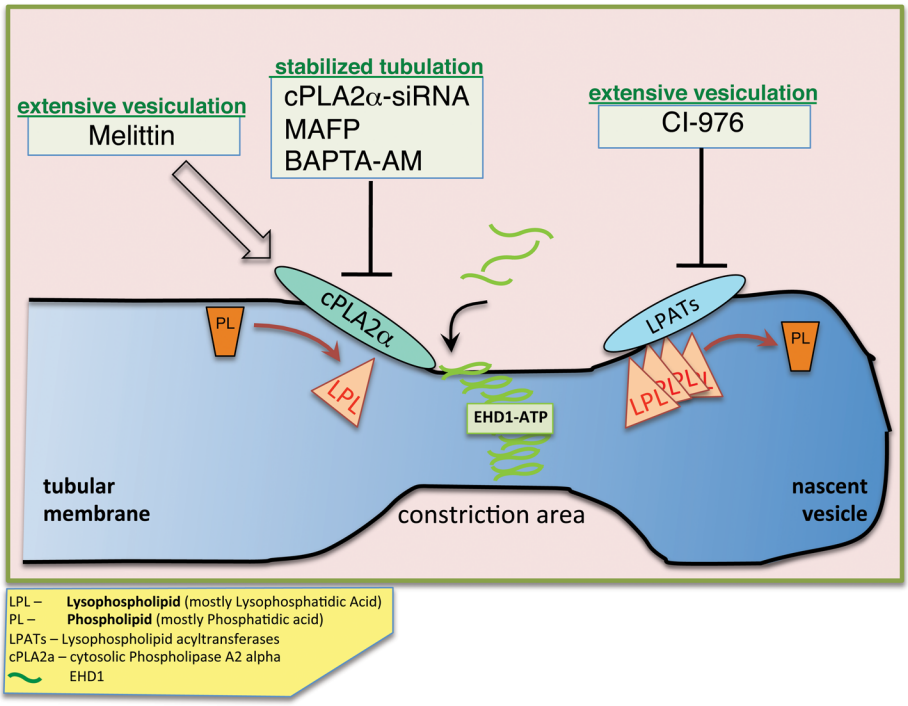

FIGURE 8: A speculative model describing cPLA2α and EHD1 function in vesiculation. cPLA2α is recruited onto the outer membrane leaflet of cholesterol-enriched endosomes containing cargo coming in from the clathrin-independent pathway. As a result, the level of LPL (mostly lysophosphatidic acid) locally increases, generating curvature and giving rise to a constricted region. Membrane-bound cPLA2α engages EHD1 via its interaction (likely in the context of a complex), and vesiculation proceeds, possibly through oligomerization of EHD1 and ATP hydrolysis. Local accumulation of LPL, either by activating cPLA2α with melittin or by inhibiting LPAT activity with CI-976, accelerates fission and vesiculation, whereas interfering with cPLA2α activity by knockdown or inhibition (with the inhibitor MAFP or the chelator BAPTA-AM) slows down vesiculation, and tubular structures are stabilized.

CD59-containing endosomes, further supporting their involvement in a "scission complex" composed of multiple proteins needed to complete fission. Accordingly, treating HeLa cells with melittin, a PLA2-activating peptide (Steiner *et al.*, 1993), generated profound vesiculation of CD59 endosomes, possibly by enhancing endogenous cPLA2α recruitment onto membranes or affecting a membrane-bound pool of the enzyme. On the other hand, overexpression of the EHD1 ΔEH mutant, which appears to induce scission in a nonregulated manner, was able to carry out intensive vesiculation of CD59- and MICAL-L1–decorated endosomes, even in the absence of cPLA2α (Figure 7).

How might the EHD1(ΔEH) mutant carry out scission in the absence of cPLA2α? EHD1 is capable of binding membranes both via its scissor-like helical regions and through its EH domain (Daumke *et al.*, 2007; Naslavsky *et al.*, 2007). In addition, EHD1(ΔEH) can still dimerize in the absence of its EH domain with either endogenous EHD1 or by homodimerization with other transfected EHD1(ΔEH) proteins. In either case, such dimers would contain lipid-binding domains that would allow them to be recruited onto membranes. Furthermore, partial compensation for cPLA2α loss might take place upon its knockdown by other lipid-shaping enzymes, as suggested by the modest effects described in the trafficking studies we have done. We therefore hypothesize that uncontrolled scission can still take place with less favorable lipid-bending requirements.

Overall, our studies identify a novel interaction between EHD1 and cPLA2α. Moreover, they support a model by which the generation of LPL by cPLA2α in certain subsets of endosomes leads to high curvature and constriction of tubular endocytic membranes, which, in concert with EHD1 and other proteins, culminates in vesicle fission.

MATERIALS AND METHODS

Recombinant DNA constructs

The cPLA2α was subcloned from GFP-cPLA2α (a kind gift of C. Leslie, National Jewish Medical and Research Center, Denver, CO). It was PCR amplified using primers ACGCGTCGACCATGTCATTTATAGATCCTTACC and CGGGGTACCCTATGCTTTGGGTTTACTTAGAAAC and cloned into a pHA-CMV vector (Clontech, Mountain View, CA), or primers GGGAATTCCATATGATGTCATTTATAGATCCTTACC and ACGCGTCGACCTATGCTTTGGGTTTACTTAGAAAC cloned into PGBKT7 vector (Clontech). The siRNA-resistant mutant of wild-type HA-cPLA2α was created with the QuikChange Kit (Stratagene, Santa Clara, CA), in which HA-cPLA2α was engineered to contain substitutions at base pairs 636 (A to G), 639 (C to T), 642 (A to G), 1065 (C to G), 1071 (T to A), 1074 (A to G), 1395 (T to A), 1398 (T to C), 1401 (T to A), 1656 (C to G), 1659 (A to T) and 1662 (T to C). All these substitutions maintain the wild-type amino acid sequence. The siRNA-resistant active-site mutant of HA-cPLA2α (S228A) was generated also with the QuikChange Kit by using siRNA-resistant wild-type HA-cPLA2α as a template. The full-length wild-type GFP-myc-EHD1 and GFP-myc-EHD1(ΔEH) were described previously (Caplan *et al.*, 2002). Cloning of the full-length HA-MICAL-L1 was described previously (Sharma *et al.*, 2009a). GFP-dynamin K44A and HA-JNK1 were kindly provided by M. McNiven (Mayo Clinic, Rochester, MN) and S. Gutkind (National Institute of Dental and Craniofacial Research, National Institutes of Health, Bethesda, MD), respectively. Tomato-EHD1 and GFP-MICAL-L1 were previously described (Sharma *et al.*, 2009a). Two-hybrid control vectors (GAL4ad-SV40 large T antigen and GAL4bd-p53) were obtained from Clontech. PGBKT7 two-hybrid vector containing MICAL-L1 and PGAD7 vector containing EHD1 were described previously (Sharma *et al.*, 2009a). Tac (the α subunit of interleukin-2 receptor) was described previously (Radhakrishna and Donaldson, 1997; Naslavsky *et al.*, 2003). The Tac-GPI chimera possesses the GPI moiety that targets it to raft and caveolae (Delahunty *et al.*, 1993) and was from J. Bonifacino (National Institutes of Health), as described previously (Naslavsky *et al.*, 2004). Tac-LL is a chimera composed of the extracellular, lumenal, and transmembrane domains of Tac and the cytoplasmic tail of the mouse CD3 containing the DKQTLL motif, which directs this molecule into clathrin-coated pits, as previously described (Naslavsky *et al.*, 2003).

Antibodies and reagents

The affinity-purified rabbit polyclonal peptide antibodies directed against the C-terminus of human EHD1 (DLPPHLVPPSKRRHE) was previously described (Caplan *et al.*, 2002). Mouse monoclonal MEM-43 antibody against CD59 was a generous gift of V. Horejsi

(Academy of Sciences of the Czech Republic, Prague, Czech Republic; Cai *et al.*, 2011). Supernatant from W6/32 hybridoma, producing antibody against MHC I, was previously described (Naslavsky *et al.*, 2003). Supernatant from hybridoma 7G7, producing antibody against Tac, was previously described (Naslavsky *et al.*, 2003). The following commercial antibodies were used in this study: mouse anti-cPLA2α (Santa Cruz Biotechnology, Santa Cruz, CA), mouse anti-HA (Covance, Berkeley, CA), mouse anti-actin and mouse anti–MICAL-L1 (Novus Biologicals, Littleton, CO), mouse anti-Rab5 and mouse anti-EEA1 (BD Transduction Laboratories, Lexington, KY), goat anti-mouse horseradish peroxidase (HRP; Jackson ImmunoResearch Laboratories, West Grove, PA), donkey anti-rabbit HRP (GE Healthcare, Piscataway, NJ), Alexa 568 goat anti-mouse and Alexa 488 goat anti-rabbit, Alexa 568 human transferrin, Alexa 405 goat anti-mouse, and Alexa 647 goat anti–mouse F(ab)2 (Invitrogen, Carlsbad, CA). Chemicals used in this study are as follows: filipin (Sigma-Aldrich, St. Louis, MO), MAFP (Biomol International, Enzo Life Sciences, Plymouth, PA), BAPTA-AM, a calcium-specific polyamino carboxylic acid (Tocris Bioscience, Ellisville, MO), melittin (Bachem, Torrance, CA), CI-976 (Sigma-Aldrich), and jasplakinolide and cytochalasin D (Bachem). The transfection reagents FuGENE HD and GeneExpresso were obtained from Roche Applied Science (Indianapolis, IN) and Excellgen (Gaithersburg, MD), respectively.

Immunoblotting

Immunoblotting was performed essentially as described previously (Cai *et al.*, 2011), Briefly, HeLa cells were harvested and lysed on ice for 15 min in buffer containing 50 mM Tris, pH 7.4, 150 mM NaCl, 1% NP40, 0.5% sodium deoxycholate, and protease inhibitor cocktail (Roche Molecular Biochemicals, Indianapolis, IN). Total protein level in the lysate was quantified by Bio-Rad protein assay (Bio-Rad Laboratories, Hercules, CA) for equal protein loading on gels in siRNA experiments. Protein samples were separated on 8% SDS–PAGE.

Duolink proximity assay

Duolink assay (Olink Bioscience, Uppsala, Sweden) detects two different proteins at a distance of <30–40 nm from one another (Soderberg *et al.*, 2006), with a modified immunofluorescent approach. In accord with the manual, HeLa cells growing on coverslips were cotransfected (16 h) with GFP-myc-EHD1 and HA-MICAL-L1, HA-cPLA2α, or HA-JNK and fixed. To ascertain that cells measured in the experiment were doubly transfected (with GFP-myc-EHD1 and HA- tagged proteins), a set of coverslips was first analyzed for coexpression with anti-HA, followed by 568 goat anti-mouse (since red and blue dyes were used to detect proximity; see later discussion). Approximately 95% of the transfected cells were doubly transfected. The parallel set of coverslips was double stained with rabbit anti-myc and mouse anti-HA antibodies for 1 h, followed by incubation with secondary antibody conjugated to PLA probe oligonucleotides. After 1 h, oligonucleotides were ligated and amplified by adding ligase and polymerase, respectively. Red fluorescently labeled probe, complementary to the amplified PLA oligonucleotides, was allowed to hybridize, and coverslips were then mounted with 4′,6-diamidino-2-phenylindole–containing mounting solution. Proximity events were detected as red dots and were counted with 127–131 cells per experiment. Three independent experiments were plotted.

Coimmunoprecipitation

HeLa cells growing in 100-mm dishes were transfected with either HA-cPLA2α or HA-JNK1 (negative control) using GeneExpresso. After 20 h, cells were lysed on ice for 1 h in buffer containing 50 mM Tris, pH 7.4, 150 mM NaCl, 0.5% Brij 98, 0.25 mM 4-(2-aminoethyl) benzenesulfonyl fluoride, 10 μM leupeptin, and 10 μM aprotinin. Cell lysates were incubated with rabbit anti-EHD1 antibodies at 4°C overnight. Rabbit IP Matrix beads (Santa Cruz Biotechnology) were added to the cell lysate–antibody mixture for 3 h at 4°C. Beads were washed four times in buffer containing 50 mM Tris, pH 7.4, 150 mM NaCl, and 0.1% Brij 98, and proteins were eluted by using 4× loading buffer (250 mM Tris, pH 6.8, 8% SDS, 40% glycerol, 5% β-mercaptoethanol, 0.2% bromophenol blue [wt/vol]). Samples were subjected to 8% SDS–PAGE, followed by blotting with anti-HA and anti-EHD1 antibodies.

Yeast two-hybrid analysis

As described previously (Naslavsky *et al.*, 2006), the *Saccharomyces cerevisiae* strain AH109 (BD Biosciences Clontech, Palo Alto, CA) was maintained on yeast extract/peptone/dextrose agar plates. Transformation was done by the lithium acetate procedure as described in the instructions for the Matchmaker Two-Hybrid Kit (BD Biosciences Clontech). For colony growth assays, AH109 cotransformants were streaked on plates lacking leucine and tryptophan and allowed to grow at 30°C, usually for 2 d, or until colonies were large enough for further assays. An average of three to four colonies was then chosen and suspended in water, equilibrated to the same optical density at 600 nm, and replated on plates lacking leucine and tryptophan (+HIS) as well as plates also lacking histidine (–HIS). After 2 d of growth, both +HIS and –HIS plates were scanned.

siRNA treatment and rescue experiments

Four specific oligonucleotides (GAUGAAGGCAUUAUACGAA, CAAGUUGGAUUCAUCGUAU, ACAGUGGGCUCACAUUUAA, and GAAAUUGGCAUGGCUAAAU) directed at human cPLA2α (On-Target SMART pool, Dharmacon, Lafayette, CO), were transfected to HeLa cells with Oligofectamine (Invitrogen) for 48 h to knock down endogenous human cPLA2α. The specificity of the knockdown was confirmed by performing siRNA treatment on cells overexpressing HA-cPLA2α detected with anti-HA antibody. For rescue experiments, either the wild-type silent HA-cPLA2α or mutant HA-cPLA2α S228A was transfected into cPLA2α-siRNA–treated cells by using GeneExpresso for 4–5 h after the start of siRNA treatment. Their expression was verified with anti-HA antibody by immunofluorescence. EHD1 knockdown was done as previously described (Cai *et al.*, 2011).

Immunofluorescence and CD59 uptake assay

HeLa cells were grown on cover slips, occasionally transfected with GeneExpresso as noted, and fixed with 4% (vol/vol) paraformaldehyde in phosphate-buffered saline (PBS) as described previously (Caplan *et al.*, 2002). Fixed cells were incubated with primary antibodies prepared in staining solution (0.2% saponin [wt/vol] and 0.5% bovine serum albumin BSA [wt/vol] in PBS) for 1 h at room temperature. After washes with PBS, cells were incubated with the appropriate fluorochrome-conjugated secondary antibody mixture in staining solution for 30 min at room temperature. All images were acquired using a Zeiss LSM 5 Pascal confocal microscope (Carl Zeiss, Jena, Germany) by using a 63×, 1.4 numerical aperture objective with appropriate filters. For CD59 uptake, cells in complete medium were incubated with anti-CD59 antibody for the indicated times at 37°C, followed by 1 min of acid stripping with 0.5 M NaCl and 0.5% acetic acid, pH 3.0, to remove surface-bound CD59 antibody. Cells were fixed after stripping and stained with appropriate secondary antibodies.

Acute manipulation of PLA2 activity

HeLa cells were either untreated or treated with pharmacological agents for various times. For the study of CD59-containing structures

with pharmacological agents by immunofluorescence, cells grown on cover slips were pretreated with either melittin for ≤30 min or MAFP and BAPTA-AM for ≤1 h, followed by 15 min of CD59 internalization in the presence of these pharmacological agents. The tubulation of CD59-containing endosomes was analyzed by confocal microscopy and quantified. For internalization studies of different Tac cargoes by flow cytometry, cells grown on plates were detached by a brief incubation with Cellstripper (Mediatech, Manassas, VA) for 2 min at 37°C and pretreated with either melittin for 30 min or MAFP and BAPTA-AM for 1 h, followed by 1 h of CD59 internalization in the presence of these agents. The internalized Tac cargoes were detected by flow cytometry. For recycling studies of different Tac cargoes by flow cytometry, cells were first pulsed with anti-Tac antibody for 1 h, followed by a chase in complete media in the presence of the pharmacological agents for 2 h. The reappearance of Tac cargoes was determined by flow cytometry.

Flow cytometry

Internalization and recycling rates of Tac-GPI, Tac, and Tac-LL were all measured by flow cytometry. HeLa cells were treated with cPLA2α-siRNA or pharmacological agents for the indicated times. Cells were detached from plates by a brief incubation with Cellstripper for 2 min at 37°C, and experiments were carried out on suspended cells. For internalization studies, suspended cells were incubated with anti-Tac antibody for 1 h in complete media at 37°C (internalized pool), followed by a 1-min acid strip to remove surface-bound antibody. After fixation, internalized anti-Tac was detected with Alexa 647–conjugated goat anti–mouse $F(ab)_2$ containing 0.2% saponin. For Tac recycling assay, suspended cells were pulsed with anti-Tac antibody for 1 h at 37°C in complete media and then stripped for 1 min and chased in complete media (37°C) for 2 h. After fixation, recycled anti-Tac (reappearing at the plasma membrane) was detected using secondary antibody without saponin. To calculate the percentage of the different Tac cargoes returning to the plasma membrane, the anti-Tac surface value was divided by the internalized pool. At least 10,000 cells/sample were collected for flow cytometry analysis (BD Biosciences, San Diego, CA).

Determination of cellular LPA levels

Extraction of LPA from cell pellets was done essentially as described (Bathena *et al.*, 2011), with acidified 1-butanol. Saturated LPA species (18:0, 16:0) and unsaturated species (18:1, 20:4) were analyzed with a Waters ACQUITY ultra-performance liquid chromatography system (Waters, Milford, MA) coupled to a 4000 Q TRAP quadrupole linear ion trap hybrid mass spectrometer with an electrospray ionization source (Applied Biosystems, MDS Sciex, Foster City, CA). The total protein was measured for each sample, and LPA concentration was expressed as ng LPA/mg protein.

ACKNOWLEDGMENTS

We thank Vaclav Horejsi and Christina Leslie for the kind gifts of reagents. We thank Parul Katoch for assistance with filipin imaging, Dawn Katafiasz for drug calibration, and especially Y. Alnouti and Sai Praneeth Bathena from the College of Pharmacy, University of Nebraska Medical Center (Omaha, NE), for their expertise in LPA measurements. This work was supported by Nebraska Center for Cell Signaling Grant 5P20GM103489-10 from the National Institute of General Medical Sciences (N.N.), Nebraska Department of Health Grant R01GM087455 from the National Institute of General Medical Sciences (S.C., N.N.), and support from a student assistantship award from the University of Nebraska Medical Center (B.C.)

REFERENCES

Bate C, Ingham V, Williams A (2011). Inhibition of phospholipase A(2) increased the removal of the prion derived peptide PrP82-146 from cultured neurons. Neuropharmacology 60, 365–372.

Bathena SP, Huang J, Nunn ME, Miyamoto T, Parrish LC, Lang MS, McVaney TP, Toews ML, Cerutis DR, Alnouti Y (2011). Quantitative determination of lysophosphatidic acids (LPAs) in human saliva and gingival crevicular fluid (GCF) by LC-MS/MS. J Pharm Biomed Anal 56, 402–407.

Bechler ME, Doody AM, Ha KD, Judson BL, Chen I, Brown WJ (2011). The phospholipase A enzyme complex PAFAH Ib mediates endosomal membrane tubule formation and trafficking. Mol Biol Cell 22, 2348–2359.

Brown WJ, Chambers K, Doody A (2003). Phospholipase A2 (PLA2) enzymes in membrane trafficking: mediators of membrane shape and function. Traffic 4, 214–221.

Cai B, Katafiasz D, Horejsi V, Naslavsky N (2011). Pre-sorting endosomal transport of the GPI-anchored protein, CD59, is regulated by EHD1. Traffic 12, 102–120.

Campelo F, Fabrikant G, McMahon HT, Kozlov MM (2010). Modeling membrane shaping by proteins: focus on EHD2 and N-BAR domains. FEBS Lett 584, 1830–1839.

Caplan S, Naslavsky N, Hartnell LM, Lodge R, Polishchuk RS, Donaldson JG, Bonifacino JS (2002). A tubular EHD1-containing compartment involved in the recycling of major histocompatibility complex class I molecules to the plasma membrane. EMBO J 21, 2557–2567.

Casas J, Gijon MA, Vigo AG, Crespo MS, Balsinde J, Balboa MA (2006). Phosphatidylinositol 4,5-bisphosphate anchors cytosolic group IVA phospholipase A2 to perinuclear membranes and decreases its calcium requirement for translocation in live cells. Mol Biol Cell 17, 155–162.

Chambers K, Judson B, Brown WJ (2005). A unique lysophospholipid acyltransferase (LPAT) antagonist, CI-976, affects secretory and endocytic membrane trafficking pathways. J Cell Sci 118, 3061–3071.

Corvera S, Chawla A, Chakrabarti R, Joly M, Buxton J, Czech MP (1994). A double leucine within the GLUT4 glucose transporter COOH-terminal domain functions as an endocytosis signal. J Cell Biol 126, 1625.

Damke H, Baba T, Warnock DE, Schmid SL (1994). Induction of mutant dynamin specifically blocks endocytic coated vesicle formation. J Cell Biol 127, 915–934.

Daumke O, Lundmark R, Vallis Y, Martens S, Butler PJ, McMahon HT (2007). Architectural and mechanistic insights into an EHD ATPase involved in membrane remodelling. Nature 449, 923–927.

de Figueiredo P, Doody A, Polizotto RS, Drecktrah D, Wood S, Banta M, Strang MS, Brown WJ (2001). Inhibition of transferrin recycling and endosome tubulation by phospholipase A2 antagonists. J Biol Chem 276, 47361–47370.

Delahunty MD, Stafford FJ, Yuan LC, Shaz D, Bonifacino JS (1993). Uncleaved signals for glycosylphosphatidylinositol anchoring cause retention of precursor proteins in the endoplasmic reticulum. J Biol Chem 268, 12017–12027.

Drecktrah D, Chambers K, Racoosin EL, Cluett EB, Gucwa A, Jackson B, Brown WJ (2003). Inhibition of a Golgi complex lysophospholipid acyltransferase induces membrane tubule formation and retrograde trafficking. Mol Biol Cell 14, 3459–3469.

Edidin M (2003). The state of lipid rafts: from model membranes to cells. Annu Rev Biophys Biomol Struct 32, 257–283.

Gagescu R, Demaurex N, Parton RG, Hunziker W, Huber LA, Gruenberg J (2000). The recycling endosome of Madin-Darby canine kidney cells is a mildly acidic compartment rich in raft components. Mol Biol Cell 11, 2775–2791.

Gaudreault SB, Chabot C, Gratton JP, Poirier J (2004). The caveolin scaffolding domain modifies 2-amino-3-hydroxy-5-methyl-4-isoxazole propionate receptor binding properties by inhibiting phospholipase A2 activity. J Biol Chem 279, 356–362.

Graham TR, Kozlov MM (2010). Interplay of proteins and lipids in generating membrane curvature. Curr Opin Cell Biol 22, 430–436.

Grimmer S, Ying M, Walchli S, van Deurs B, Sandvig K (2005). Golgi vesiculation induced by cholesterol occurs by a dynamin- and cPLA2-dependent mechanism. Traffic 6, 144–156.

Harte RA, Yeaman SJ, Jackson B, Suckling KE (1995). Effect of membrane environment on inhibition of acyl-CoA:cholesterol acyltransferase by a range of synthetic inhibitors. Biochim Biophys Acta 1258, 241–250.

Hurley JH (2010). The ESCRT complexes. Crit Rev Biochem Mol Biol 45, 463–487.

Hurley JH, Hanson PI (2010). Membrane budding and scission by the ESCRT machinery: it's all in the neck. Nat Rev Mol Cell Biol 11, 556–566.

Ivanova PT, Cerda BA, Horn DM, Cohen JS, McLafferty FW, Brown HA (2001). Electrospray ionization mass spectrometry analysis of changes in phospholipids in RBL-2H3 mastocytoma cells during degranulation. Proc Nat Acad Sci USA 98, 7152–7157.
Jaiswal JK, Rivera VM, Simon SM (2009). Exocytosis of post-Golgi vesicles is regulated by components of the endocytic machinery. Cell 137, 1308–1319.
Jakobsson J, Ackermann F, Andersson F, Larhammar D, Low P, Brodin L (2011). Regulation of synaptic vesicle budding and dynamin function by an EHD ATPase. J Neurosci 31, 13972–13980.
Kessels MM, Dong J, Leibig W, Westermann P, Qualmann B (2006). Complexes of syndapin II with dynamin II promote vesicle formation at the *trans*-Golgi network. J Cell Sci 119, 1504–1516.
Klapisz E, Masliah J, Bereziat G, Wolf C, Koumanov KS (2000). Sphingolipids and cholesterol modulate membrane susceptibility to cytosolic phospholipase A(2). J Lipid Res 41, 1680–1688.
Kooijman EE, Chupin V, de Kruijff B, Burger KN (2003). Modulation of membrane curvature by phosphatidic acid and lysophosphatidic acid. Traffic 4, 162–174.
Kooijman EE, Chupin V, Fuller NL, Kozlov MM, de Kruijff B, Burger KN, Rand PR (2005). Spontaneous curvature of phosphatidic acid and lysophosphatidic acid. Biochemistry 44, 2097–2102.
Lamaze C, Dujeancourt A, Baba T, Lo CG, Benmerah A, Dautry-Varsat A (2001). Interleukin 2 receptors and detergent-resistant membrane domains define a clathrin-independent endocytic pathway. Mol Cell 7, 661–671.
Lenz M, Morlot S, Roux A (2009). Mechanical requirements for membrane fission: common facts from various examples. FEBS Lett 583, 3839–3846.
Lewis V, Hooper NM (2011). The role of lipid rafts in prion protein biology. Front Biosci 16, 151–168.
Llorente A, van Deurs B, Sandvig K (2007). Cholesterol regulates prostasome release from secretory lysosomes in PC-3 human prostate cancer cells. Eur J Cell Biol 86, 405–415.
Madshus IH, Sandvig K, Olsnes S, van Deurs B (1987). Effect of reduced endocytosis induced by hypotonic shock and potassium depletion on the infection of Hep 2 cells by picornaviruses. J Cell Physiol 131, 14–22.
Massol RH, Larsen JE, Kirchhausen T (2005). Possible role of deep tubular invaginations of the plasma membrane in MHC-I trafficking. Exp Cell Res 306, 142–149.
Maxfield FR, Wustner D (2002). Intracellular cholesterol transport. J Clin Invest 110, 891–898.
Mayor S, Riezman H (2004). Sorting GPI-anchored proteins. Nat Rev Mol Cell Biol 5, 110–120.
Mayor S, Sabharanjak S, Maxfield FR (1998). Cholesterol-dependent retention of GPI-anchored proteins in endosomes. EMBO J 17, 4626–4638.
Mesaki K, Tanabe K, Obayashi M, Oe N, Takei K (2011). Fission of tubular endosomes triggers endosomal acidification and movement. PLoS One 6, e19764.
Montesano R, Roth J, Robert A, Orci L (1982). Non-coated membrane invaginations are involved in binding and internalization of cholera and tetanus toxins. Nature 296, 651–653.
Moya M, Dautry-Varsat A, Goud B, Louvard D, Boquet P (1985). Inhibition of coated pit formation in Hep2 cells blocks the cytotoxicity of diphtheria toxin but not that of ricin toxin. J Cell Biol 101, 548–559.
Naslavsky N, Rahajeng J, Chenavas S, Sorgen PL, Caplan S (2007). EHD1 and Eps15 interact with phosphatidylinositols via their Eps15 homology domains. J Biol Chem 282, 16612–16622.
Naslavsky N, Rahajeng J, Sharma M, Jovic M, Caplan S (2006). Interactions between EHD proteins and Rab11-FIP2: a role for EHD3 in early endosomal transport. Mol Biol Cell 17, 163–177.
Naslavsky N, Weigert R, Donaldson JG (2003). Convergence of non-clathrin- and clathrin-derived endosomes involves Arf6 inactivation and changes in phosphoinositides. Mol Biol Cell 14, 417–431.
Naslavsky N, Weigert R, Donaldson JG (2004). Characterization of a non-clathrin endocytic pathway: membrane cargo and lipid requirements. Mol Biol Cell 15, 3542–3552.
Prinz WA, Hinshaw JE (2009). Membrane-bending proteins. Crit Rev Biochem Mol Biol 44, 278–291.
Puthenveedu MA, Lauffer B, Temkin P, Vistein R, Carlton P, Thorn K, Taunton J, Weiner OD, Parton RG, von Zastrow M (2010). Sequence-dependent sorting of recycling proteins by actin-stabilized endosomal microdomains. Cell 143, 761–773.
Radhakrishna H, Donaldson JG (1997). ADP-ribosylation factor 6 regulates a novel plasma membrane recycling pathway. J Cell Biol 139, 49–61.
Reverter M *et al.* (2011). Cholesterol transport from late endosomes to the Golgi regulates t-SNARE trafficking, assembly and function. Mol Biol Cell 22, 4108–4123.
Romer W *et al.* (2007). Shiga toxin induces tubular membrane invaginations for its uptake into cells. Nature 450, 670–675.
Romer W *et al.* (2010). Actin dynamics drive membrane reorganization and scission in clathrin-independent endocytosis. Cell 140, 540–553.
Roux A, Uyhazi K, Frost A, De Camilli P (2006). GTP-dependent twisting of dynamin implicates constriction and tension in membrane fission. Nature 441, 528–531.
Sabharanjak S, Sharma P, Parton RG, Mayor S (2002). GPI-anchored proteins are delivered to recycling endosomes via a distinct cdc42-regulated, clathrin-independent pinocytic pathway. Dev Cell 2, 411–423.
San Pietro E *et al.* (2009). Group IV phospholipase A(2)alpha controls the formation of inter-cisternal continuities involved in intra-Golgi transport. PLoS Biol 7, e1000194.
Sandvig K, Torgersen ML, Raa HA, van Deurs B (2008). Clathrin-independent endocytosis: from nonexisting to an extreme degree of complexity. Histochem Cell Biol 129, 267–276.
Sandvig K, van Deurs B (1994). Endocytosis and intracellular sorting of ricin and Shiga toxin. FEBS Lett 346, 99–102.
Sharma M, Giridharan SS, Rahajeng J, Naslavsky N, Caplan S (2009a). MICAL-L1 links EHD1 to tubular recycling endosomes and regulates receptor recycling. Mol Biol Cell 20, 5181–5194.
Sharma M, Jovic M, Kieken F, Naslavsky N, Sorgen P, Caplan S (2009b). A model for the role of EHD1-containing membrane tubules in endocytic recycling. Commun Integr Biol 2, 431–433.
Sharma P, Varma R, Sarasij RC, Ira, Gousset K, Krishnamoorthy G, Rao M, Mayor S (2004). Nanoscale organization of multiple GPI-anchored proteins in living cell membranes. Cell 116, 577–589.
Sharp JD *et al.* (1994). Serine 228 is essential for catalytic activities of 85-kDa cytosolic phospholipase A2. J Biol Chem 269, 23250–23254.
Shin N, Ahn N, Chang-Ileto B, Park J, Takei K, Ahn SG, Kim SA, Di Paolo G, Chang S (2008). SNX9 regulates tubular invagination of the plasma membrane through interaction with actin cytoskeleton and dynamin 2. J Cell Sci 121, 1252–1263.
Soderberg O *et al.* (2006). Direct observation of individual endogenous protein complexes in situ by proximity ligation. Nat Methods 3, 995–1000.
Staneva G, Angelova MI, Koumanov K (2004). Phospholipase A2 promotes raft budding and fission from giant liposomes. Chem Phys Lipids 129, 53–62.
Steiner MR, Bomalaski JS, Clark MA (1993). Responses of purified phospholipases A2 to phospholipase A2 activating protein (PLAP) and melittin. Biochim Biophys Acta 1166, 124–130.
van der Bliek AM, Redelmeier TE, Damke H, Tisdale EJ, Meyerowitz EM, Schmid SL (1993). Mutations in human dynamin block an intermediate stage in coated vesicle formation. J Cell Biol 122, 553–563.